Check for updates

Cryospheric Impacts on Volcano-Magmatic Systems

Benjamin R. Edwards[1]*, James K. Russell[2] and Meagen Pollock[3]

[1]Department of Earth Sciences, Dickinson College, Carlisle, PA, United States, [2]Earth, Ocean, and Atmospheric Sciences, University of British Columbia, Vancouver, BC, Canada, [3]Department of Earth Sciences, College of Wooster, Wooster, OH, United States

In contrast to water and air, ice is the most dynamic enveloping medium and unique environment for volcanic eruptions. While all three environments influence volcanic activity and eruption products, the cryospheric eruption environment is unique because: 1) it supports rapid changes between those environments (i.e. subglacial, subaqueous, subaerial), 2) it promotes a wide range of eruption styles within a single eruption cycle (explosive, effusive), 3) it creates unique edifice-scale morphologies and deposits, and 4) it can modulate the timing and rates of magmatism. The distinctive products of cryospheric eruptions offer a robust means of tracking paleoclimate changes at the local, regional and global scale. We provide a framework for understanding the influence of the cryosphere on glaciovolcanic systems, landforms and deposits.

INTRODUCTION

Volcanic systems have many ways of recording and responding to variations in their eruptive environments. As early as the 1800s pillow basalts were speculated to form during eruptions of lava in water (*aquatic environment*; cf. Lewis, 1904)—an assumption that was not confirmed by observation until the 1970s (Moore, 1970; Walker, 1992). In the early 1900s, volcanic deposits with abundant palagonite and associated with glacial sediments were suggested to have formed within a *cryospheric environment* (the Palagonite/Mobérg Formation of Iceland: Peacock, 1926; the Tuya Formation in British Columbia, Canada: Kerr, 1948, 1940; Mathews, 1947). In contrast, the first written detailed description of an explosive *subaerial* eruption dates back to at least 79 AD (Pliny the Younger, 2014), and the majority of our observations are from this environment, for which abundant diagnostic criteria exist. For example, deposits of airfall tephra typically drape the entire landscape and lavas flow unimpeded except by local topography.

Forensic volcanological studies are increasingly able to use volcanic stratigraphy to track dynamic changes in environmental conditions attending volcanic eruptions. For example, Russell et al. (2021) mapped variations in the elevations of passages zones preserved in 1.9 Ma glaciovolcanic deposits that recorded transitions from aquatic to subaerial depositional environments. They used these stratigraphic relationships to reconstruct transient fluctuations in the height and depth of the syn-eruption englacial lake that occurred on time-scales of days to weeks to months. Future studies of eruptions and deposits from the cryospheric environment will increasingly be key for reconstructing and tracking changes in Earth's climate that have occurred over the last 3 Ma or more (Smellie and Edwards, 2016; Smellie, 2018).

All three environments (i.e. air, water, ice) dictate styles of eruption, edifice morphologies, and the distribution and nature of volcanic lithofacies. For the purposes of this work, we consider: the *subaerial environment* as dominated by air at Earth's surface under standard conditions (25 C, 0.101

TABLE 1 | Important physical parameters of eruption environment media.

Environment	Subaerial (Air)	Aquatic (Water)	Cryospheric (Ice)
Factor			
Viscosity of Medium	1.81×10^{-5} Pa-s	89×10^{-5} Pa-s	1×10^{12} Pa-s
Density of Medium	1.225 kg m^{-3}	1,020 kg m^{-3}	921 kg m^{-3}
Environmental Vertical Pressure (EVP) Exerted at Vent	~0.1 MPa (at sea level at 25°C)	20–30 MPa (MOR; 2–3 km below sea level)	~7 MPa (Vatnajökull; 850 m)
		50 MPa (abyssal plain; 5 km b.s.L.)	~32 MPa (EAIS; 3.5 km)
Potential Change in EVP During Eruption	0	0	7–32 MPa
Potential Change in EVP During System Life Cycle	0	2 MPa (200 m of sea level change max.)	7–32 MPa (full deglaciation)
Thermal Diffusivity	20×10^{-6} m^2 s^{-1}	0.14×10^{-6} m^2 s^{-1}	1×10^{-6} m^2 s^{-1}
Thermal Conductivity	0.025 W m^{-1} K^{-1}	0.6 W m^{-1} K^{-1}	2.2 W m^{-1} K^{-1}
Heat Capacity	1.0 kJ kg^{-1} K^{-1}	4.18 kJ kg^{-1} K^{-1}	2.0 kJ kg^{-1} K^{-1}
h value (heat transfer coefficient)	2.5–500 W m^{-2} K^{-1} [free to forced convection]	100–25,000 W m^{-2} K^{-1}	0
Thermal Energy for Phase Change	0	2.3×10^6 kJ m^{-3} (liquid to gas)	0.31×10^6 kJ m^{-3} (solid to liquid)
Total Potential Thermal Energy Loss To Convert Environment to Gas at 100°C	0.12×10^3 kJ m^{-3}	$5,000.0 \times 10^3$ kJ m^{-3}	$5,300.0 \times 10^3$ kJ m^{-3}

MPa; **Table 1**); the *aquatic environment* as dominated by sea water or freshwater with essentially uniform properties (e.g., Cas and Simmons, 2018; **Table 1**); and the *cryospheric environment* as dominated by glacial ice but also including permafrost and seasonal snow pack (**Figure 1**; Edwards et al., 2020; Curtis and Kyle, 2017). While much of what is reviewed here applies to those parts of the cryosphere, the focus of this contribution is on cryospheric ice. The first two environments (i.e. subaerial/ aquatic) are well understood and have been the subject of numerous other reviews (see Cas and Simmons, 2018, for the aquatic environment). Thus, the focus of our work here is summarizing how the cryospheric environment affects volcano-magmatic systems. We provide a framework for understanding the influences of the cryosphere on (glacio) volcanic systems, landforms and deposits in contrast to the other two environments. We have expanded the review of environmental physical properties for subaerial and aqueous environments of Cas and Simmons (2018) to include the cryospheric environment. Our compilation and analysis highlight the unique impacts of the cryosphere on igneous systems, including the potential for: 1) modulating the timing and rates of magmatism, 2) creating unique edifice-scale morphologies, 3) controlling eruption processes, and 4) restricting emplacement and deposition of unique volcanic products.
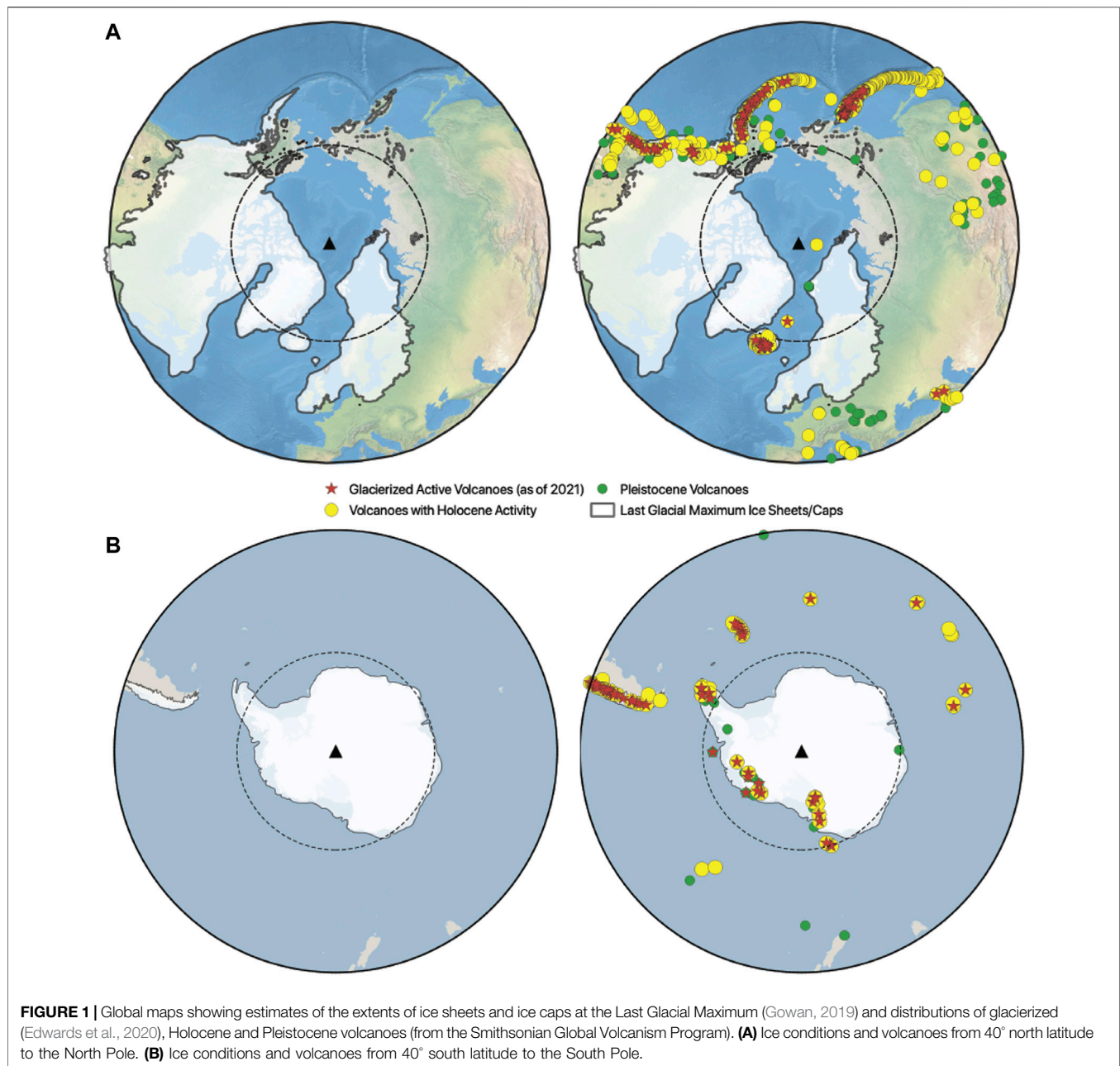
PHYSICAL CONSTRAINTS IMPOSED BY ERUPTION ENVIRONMENTS

The most obvious physical difference between the subaerial, aquatic and cryospheric environments is the medium into which an eruption occurs: air, water, or ice (and resulting meltwater), respectively. A summary of key physical parameters characteristic of these three environments (**Table 1**) shows that the *cryospheric environment* is the most extreme and the most dynamic. Melting of the

enveloping ice can cause rapid changes in eruptive pressure at the vent and melting of ice and heating of meltwater allows for efficient heat transfer and loss from the volcanic system.

The rheological properties of the enveloping media for the three environments are very different. Viscosities vary by at least one order of magnitude (air versus water), and up to 17 orders of magnitude (air versus ice). On the time scales of volcanic eruption, however, the cryospheric environment presents a viscoelastic envelope that can melt and/or flow, or fail brittley. This rheological difference in environment directly controls the distribution of explosive and effusive deposits resulting from glaciovolcanic eruptions. For example, whereas subaerial and aquatic environments allow for relatively unimpeded flow of lavas (e.g., Gregg and Fornari, 1997), cryospheric environments limit the aerial distribution of lavas by imposing physical barriers, even though snow and ice can support the mass of flowing lava over short time-scales (e.g., 24 h or less; Edwards et al., 2012, 2013, 2015). In explosive eruptions, the enveloping media strongly controls the distribution of volcanic ash; large subaerial eruptions can produce global distributions of tephra and water can distribute tephra rafts across ocean basins, while cryospheric environments can, although do not always, restrict ash dispersal because ash frequently ash is deposited in cavities within the ice or in the englacial lake (e.g., Jude-Eton et al., 2012), and transport on the ice surface will be slow. For eruptions through very thin cryosphere, such as snowpack, dispersal may not be restricted at all.

Density differences in the surrounding media translate into substantial differences in environmental vent pressures (EVP). Depending on the depth of water or thickness of overlying ice EVP can be ~2 orders of magnitude higher in aquatic and cryospheric environments than subaerial ones (**Table 1**), which potentially suppresses expansion of volatile phases and subsequently influences fragmentation and the distribution of tephra relative to subaerial environments (cf. Cas and Simmons, 2018). For subaerial and aqueous environments, EVPs are

FIGURE 1 | Global maps showing estimates of the extents of ice sheets and ice caps at the Last Glacial Maximum (Gowan, 2019) and distributions of glacierized (Edwards et al., 2020), Holocene and Pleistocene volcanoes (from the Smithsonian Global Volcanism Program). **(A)** Ice conditions and volcanoes from 40° north latitude to the North Pole. **(B)** Ice conditions and volcanoes from 40° south latitude to the South Pole.
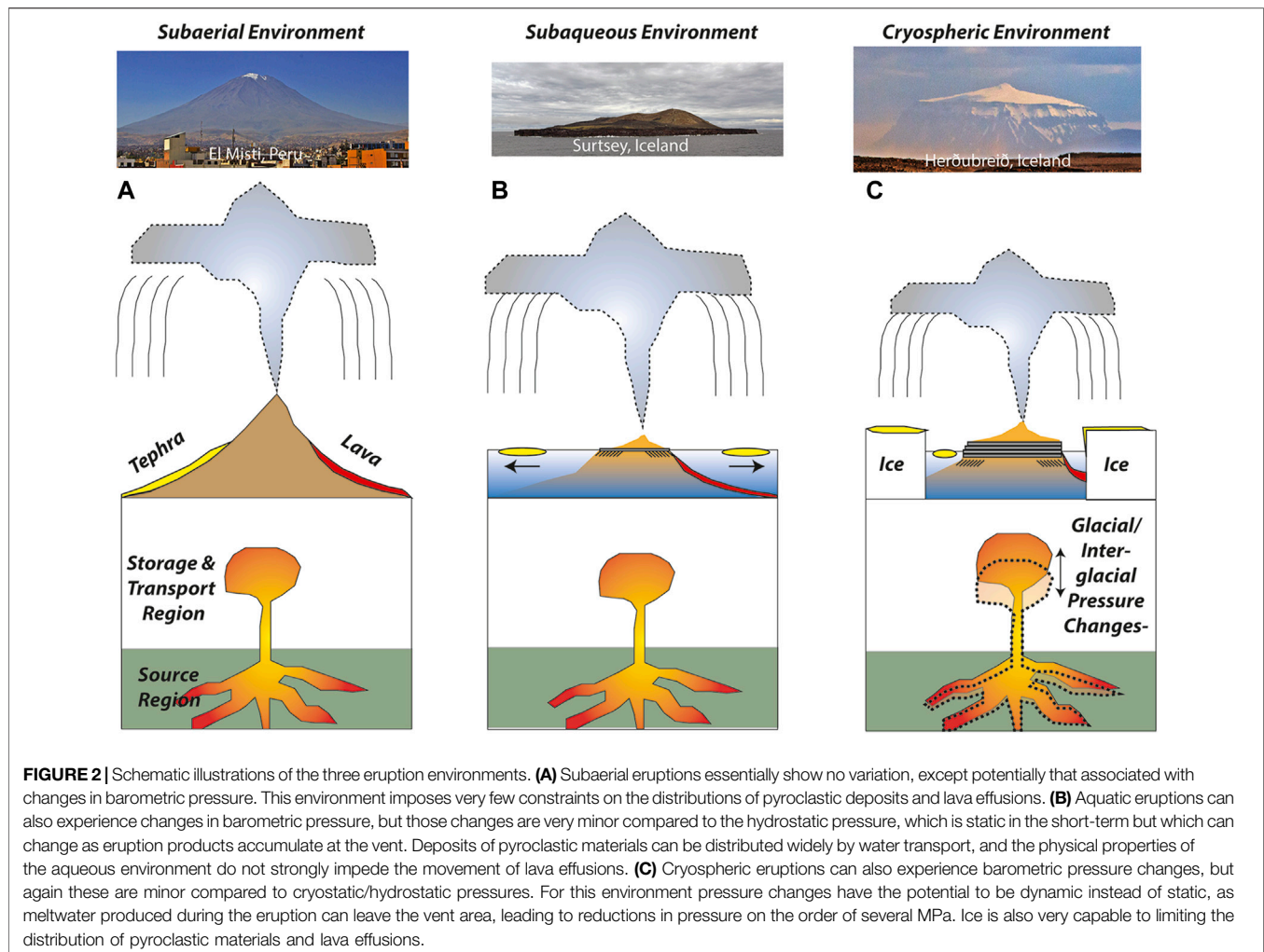
essentially static during eruptions while for cryospheric environments EVP can be dynamic and can vary by one to two orders of magnitude during the eruption as the enclosing ice melts and the resulting meltwater drains (**Figure 2**; **Table 1**).

The three environments also dissipate heat in very different ways and with different efficiencies. Conductive heat loss to the enveloping media depends on the associated physical properties. Thermal conductivity (K) reflects the materials' ability to conduct heat in a thermal gradient. Air is the most insulatory (lowest K) and is one order of magnitude lower than water and 2 orders of magnitude less than ice. Thermal diffusivity (κ) values dictate characteristic rates of heat transfer through the media, and values of κ for air are 2 orders of magnitude higher than for water and 1

order higher than for ice (**Table 1**). The lower viscosities of air and water, relative to ice, mean that heat transfer in those environments is likely to be dominated by advective heat transfer. The heat transfer coefficient, which is a simplified proxy for the complexities of advective heat transfer processes, is significantly higher for water than for air (**Table 1**). In the cryospheric environment, meltwater is rapidly produced by melting of the enclosing ice at which point advective heat transfer will dominate.

Heat in the volcanic system is also dissipated by endothermic phase transitions that attend aquatic and cryospheric eruptions. As an example, for an eruption to convert its enveloping medium to a gas phase at 100°C requires 0.12×10^3 kJ m^{-3} for air, 5,000.0

FIGURE 2 | Schematic illustrations of the three eruption environments. **(A)** Subaerial eruptions essentially show no variation, except potentially that associated with changes in barometric pressure. This environment imposes very few constraints on the distributions of pyroclastic deposits and lava effusions. **(B)** Aquatic eruptions can also experience changes in barometric pressure, but those changes are very minor compared to the hydrostatic pressure, which is static in the short-term but which can change as eruption products accumulate at the vent. Deposits of pyroclastic materials can be distributed widely by water transport, and the physical properties of the aqueous environment do not strongly impede the movement of lava effusions. **(C)** Cryospheric eruptions can also experience barometric pressure changes, but again these are minor compared to cryostatic/hydrostatic pressures. For this environment pressure changes have the potential to be dynamic instead of static, as meltwater produced during the eruption can leave the vent area, leading to reductions in pressure on the order of several MPa. Ice is also very capable to limiting the distribution of pyroclastic materials and lava effusions.

$\times 10^3$ kJ m^{-3} for water, and $5,300.0 \times 10^3$ kJ m^{-3} for ice, including the phase transitions from ice to water, and from water to steam. In the aqueous environment, about half of the required energy is used to heat water from initial temperatures, here assumed to 0°C although they could be as low as −4°C for abyssal marine environments, to phase transition temperatures for the liquid: gas/fluid transition that depend on pressure (i.e. water depth). In cryospheric environments the temperatures in the vent area will be close to the temperature for ice:water phase transition (∼0°C); even polar ice is generally at temperatures above −60°C (Cuffey and Paterson, 2010). However, the environmental medium (i.e. ice) can pass through two phase transitions via melting and vaporization, consuming the largest amount of energy per cubic meter of erupted material (**Table 1**). The differences in thermal properties are responsible for many of the macro- and microscopic differences seen in deposits from the water- and ice-dominated eruption environments, relative to subaerial volcanic deposits. As developed below, the physical conditions of the cryosphere, relative to the subaerial and aquatic environments, produce signatory characteristics at volcanoes and in their deposits, which has led to a new subdiscipline known simply as "glaciovolcanism" (Kelman et al., 2002;

Smellie, 2009; Edwards et al., 2014; Russell et al., 2014; Smellie and Edwards, 2016)

CRYOSPHERIC IMPACTS ON MAGMA GENERATION AND MIGRATION

The cryosphere (**Figure 3**) perturbs magmatic systems mainly during interstadial and interglacial periods, when ice thickness is changing and influencing lithostatic stress conditions (Andrew and Gudmundsson, 2007; Geyer and Bindeman, 2011). Static ice is no different than any other kind of lithospheric load, although compared to typical sediments or other surficial deposits, ice is about 50–70 percent less dense and is susceptible to higher rates of removal. Land-based accumulation of ice, glaciers and ice sheets operates on time scales of tens of thousands of years based on Pleistocene proxies for global sea level and ocean temperatures (e.g., Lisiecki and Raymo, 2005). However, those same records are interpreted to suggest that deglaciations happen much more rapidly. The Laurentide, Cordilleran and Svennoscandian ice sheets are all thought to have been at least 2 km thick (e.g., Clague and Ward, 2011; Lambeck et al., 2006), while at the Last
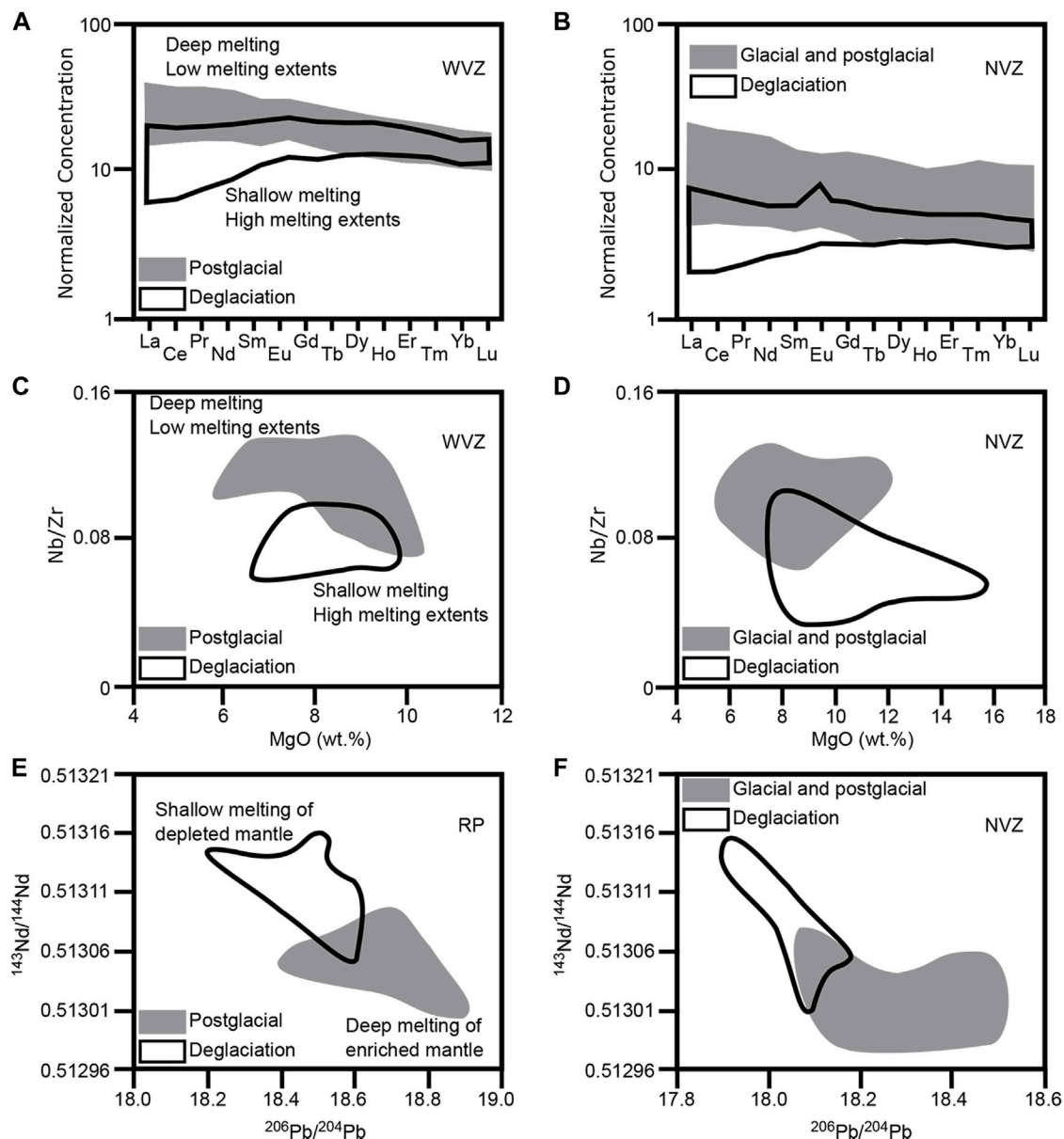
FIGURE 3 | Geochemical trends in lavas erupted during deglaciation compared to isostatic ice conditions. Deglaciation causes increased melting at shallow depths, generating melts that are depleted in Rare Earth Elements (REE), ratios of incompatible elements, and isotopes. **(A,B)** REE normalized to primitive mantle (McDonough and Sun, 1995) for Iceland's Western Volcanic Zone (WVZ; **(A)** and Northern Volcanic Zone (NVZ; **(B)**. **(C,D)** Trace element ratios as a function of MgO (wt %) for the WVZ **(C)** and NVZ **(D)**. **(E,F)** Nd and Pb isotopes for the Reykjanes Peninsula (RP; **(E)** and NVZ **(F)**. Gray fields represent lavas erupted during isostatic ice conditions (glacial and postglacial). Open fields represent lavas erupted during deglaciation. NVZ REE, trace element, and MgO data from Theistareykir from the compilation of Maclennan et al. (2002 and references in their Table 2, excluding picrites) NVZ isotope data from Theistareykir from the compilation of Sims et al. (2013 and references in their Table 1). WVZ REE, trace element, and MgO data from the compilation of Eason et al. (2015 and references in their Figure 4). RP isotope data from Gee et al. (1998).

Glacial Maximum the Icelandic ice sheet was at least 1 km thick on average (Hubbard et al., 2006; Le Breton et al., 2010). Those thicknesses were achieved over a period of ~90 ka suggesting an average accumulation rate of about 0.02 m per year. To generate a similar lithostatic load from sedimentation requires accumulation rates of about 0.01 m per year, or from volcanic activity about 0.009 m per year. In contrast, full destruction of those ice sheets

seems to take place in less than 20 ka, and likely closer to 10 ka (Lambeck et al., 2014). Those time-scales suggest ice sheet "erosion" rates about one order of magnitude larger than the accumulation rates (~0.1 m per year). These "ablation rates" are significantly higher than those typically assigned to rates of erosion for most terrestrial environments (e.g., 0.0004 m/yr; Ferrier et al., 2007), or for rates of sea level rise during

deglaciations (e.g., 0.01–0.04 m per year after the Last Glacial Maximum; Lambeck et al., 2006). After some lag time following rapid interglacial sea level rise, high strain rates combine with increased lithospheric loads to induce crustal stress regimes that suppress dike initiation and cause eruptions to cease in marine-dominated environments (Satow et al., 2021). Thus, the characteristic slow loading rate and more rapid unloading rate of ice sheets can also be expected to impact magma source regions in glacial environments by altering the lithospheric stress conditions, influencing the depths and extents of melting, magma transport and storage processes, and pressure and temperature conditions of magma evolution (e.g., crystallization, devolatilization).

For areas where decompression melting is prominent like Iceland, lithospheric unloading has been suggested to change conditions within the mantle melting region and to produce distinctive geochemical signatures (Jull and McKenzie, 1996; Gee et al., 1998; Slater et al., 1998; Maclennan et al., 2002; Sinton et al., 2005; Sims et al., 2013; Eason and Sinton, 2015; Eksinchol et al., 2019). Compared to lavas erupted during isostatic ice conditions, lavas erupted during deglaciation tend to be depleted in radiogenic isotopes and incompatible trace elements (**Figure 3**). Geochemical modeling has shown that the extent of isotopic and incompatible element depletion observed in interglacial lavas cannot be explained by changes in magma chamber processes or mantle source composition (e.g., Maclennan et al., 2002). Instead, the geochemical trends are consistent with increased mantle melting and magma ascent rates from the shallow, isotopically and incompatible element-depleted part of the mantle (Harðarson and Fitton, 1991; Jull and McKenzie, 1996; Slater et al., 1998; Eksinchol et al., 2019). In some locations, the shift in melting conditions is also recorded in major element variations (Eason and Sinton, 2015). An additional impact of deglaciation on major elements, and other parameters controlled by crustal magmatic differentiation processes, can be expected because of the effects of unloading on crustal magma transport (Wilson and Russell, 2020). Rapid deglaciation creates local stress fields favorable for dike propagation, with the potential for erupting variably evolved magmas from a range of crustal depths (Wilson and Russell, 2020).

In volcanic arcs, the effects of glaciation on eruptive chemistry and volcanic output are more likely to be driven by changes in crustal stress and rheological conditions (Geyer and Bindeman, 2011). Several different groups have suggested that hydrothermal alteration weakens host rock and glacial loading and unloading produce changes in the crustal lithosphere stress field that inhibit or drive magma storage and transport (e.g., Jellinek et al., 2004; Geyer and Bindeman, 2011; Praetorius et al., 2016; Rawson et al., 2016; Wilson and Russell, 2020). Over long time-scales crustal loading may impede dyke formation and enhance sill production, while unloading favors dyke formation and enhances magma transport into the eruption region (Gudmundsson, 1986; Sigvaldason et al., 1992; Gee et al., 1998; Glazner et al., 1999; McLeod and Tait, 1999; Jellinek and DePaolo, 2003; Jellinek et al., 2004; Andrew and Gudmundsson, 2007; Albino et al., 2010; Wilson and Russell, 2020). The cyclic loading and unloading of ice ages can lead to "glacial pumping in magma-charged lithosphere" (Edwards and

Russell, 2002; Wilson and Russell, 2020). Over short time-scales, the local stress field induced by the overlying ice sheet may interact with dyke orientation to enhance or reduce eruptive activity, thereby influencing crustal magma storage capacity (Hooper et al., 2011). Extended crustal residence times enhance magmatic differentiation by crystallization, assimilation, and mixing processes, thereby recording glaciation-driven events in lava geochemistry (Edwards et al., 2002; Asmerom et al., 2005; Wilson and Russell, 2020).

For magmas that are already close to a state of volatile saturation, rapid changes in lithospheric pressures during interstadial periods and deglaciations are of a magnitude that could drive vesiculation (Bindeman et al., 2010; Geyer and Bindeman, 2011). Sudden load removal caused by volcanic edifice destabilization and catastrophic flank collapse can force the system into a two-phase state, (Capra, 2006; Tormey, 2010; Capra et al., 2015). Rapid gravitational failure and volatile exsolution can potentially trigger an eruption or at the very least increase the eruptibility of the magma (Bindeman et al., 2010; Geyer and Bindeman, 2011; Sparks and Cashman, 2017). Separation of a volatile phase also can change the stability of crystallizing phases, and so the dynamicity of the cryospheric environment has the potential to indirectly alter the liquid line of descent for pre-existing magmas.

CRYOSPHERIC IMPACTS ON VOLCANO MORPHOLOGY

The imprint (**Figure 4**) of the cryospheric eruption environment is most visible and iconic at the edifice scale (**Figure 4**). Entire volcanoes in many parts of the world owe their distinctive morphologies to eruptions within ice while others have a more subtle morphological imprint including: anomalously steep cliffs of ice-dammed (i.e. overthickened) lavas, inverted topography caused by lava emplacement within ice-confined valleys, and characteristic resurfacing and reshaping of edifices due to ice erosion and buttress-destabilization (**Figure 4**). The morphology of tuyas and other cryospherically constrained volcanic edifices has been discussed in detail by several authors (Hickson, 2000; Smellie, 2009, 2018; Pedersen and Grosse, 2014; Russell et al., 2014; Pedersen, 2016), so here we only review the main elements that can be diagnostic of cryospheric environments.

Tuyas, less commonly referred to as "stapi" and "table mountains," are volcanoes whose overall morphology is a direct result of eruptions within confining ice (e.g., Mathews, 1947; Smellie, 2009; Pedersen and Grosse, 2014; Russell et al., 2014). These volcanic landforms have three distinct morphologies: 1) flat-topped platforms comprising laterally continuous, subhorizontal lavas commonly capping subaqueous lava-fed deltas (**Figure 4A**), 3) conical masses comprising palagonitized tephra and intrusions (**Figure 4B**), or 3) elongate ridges of subaqueous tephra and pillow lava (**Figure 4C**). A limited number of compound tuyas have been identified, particularly in British Columbia (**Figure 4D**). There, Kima'Kho tuya features a tephra cone onlapped by a platform of dipping beds of pillow lava breccias capped by horizontal sheets
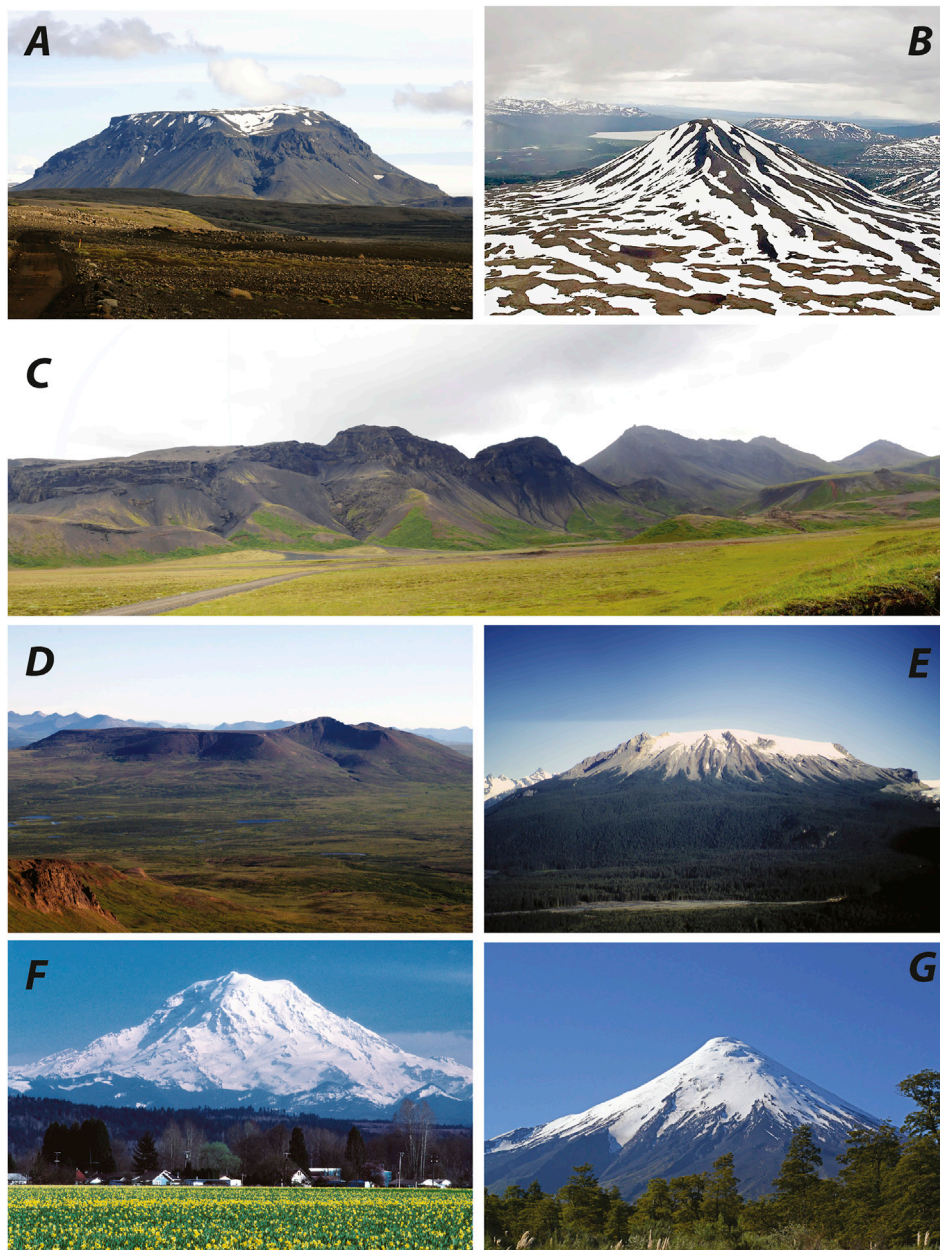
FIGURE 4 | Volcano morphologies diagnostic of cryospheric eruption environments. **(A)** Hlödufell, a flat-topped, basaltic tuya in the Western Volcanic Zone, Iceland. **(B)** South tuya, a conical, basaltic tuya in the Tuya area, British Columbia, Canada. **(C)** Kalfstindar, a basaltic tindar (a.k.a. linear tuya) in the Western Volcanic Zone, Iceland. **(D)** Kima 'Kho tuya, a compound, basaltic tuya on the Kawdy Plateau, British Columbia, Canada. **(E)** Hoodoo Mountain, a long-lived trachyte-phonolite tuya/stratovolcano, Coast Mountains, British Columbia, Canada. **(F)** Mount Rainier, an andesitic stratovolcano in the Cascade volcanic arc, Washington State, U.S.A. (Image courtesy of U.S.G.S. Cascade Volcano Observatory). **(G)** Osorno volcano, a basaltic stratovolcano in the Southern Andean Volcanic Zone, Chile. Unless specifically noted, all images in this and subsequent figures were taken by B. Edwards.

of lava (e.g., Mathews, 1947; Russell et al., 2021). Russell et al. (2014) advocated using the term "tuya" as a generic term to encompass all three morphologies and their combinations, while other authors have more nuanced views (e.g., Smellie, 2009). Recognition of these morphological elements as being unique to the cryospheric eruption environment has been critical for inferring the thicknesses and extents of paleo-ice-sheets on

Earth and on Mars (Smellie and Edwards, 2016; Edwards et al., 2020). However, the unexamined assumption that a flat-topped volcano defines a cryospheric environment is problematical especially on not-yet-visited planets. At least in shallow water, the aquatic eruption environment can produce similar morphologies, with the best example being Surtsey volcano, located off the coast of south Iceland.
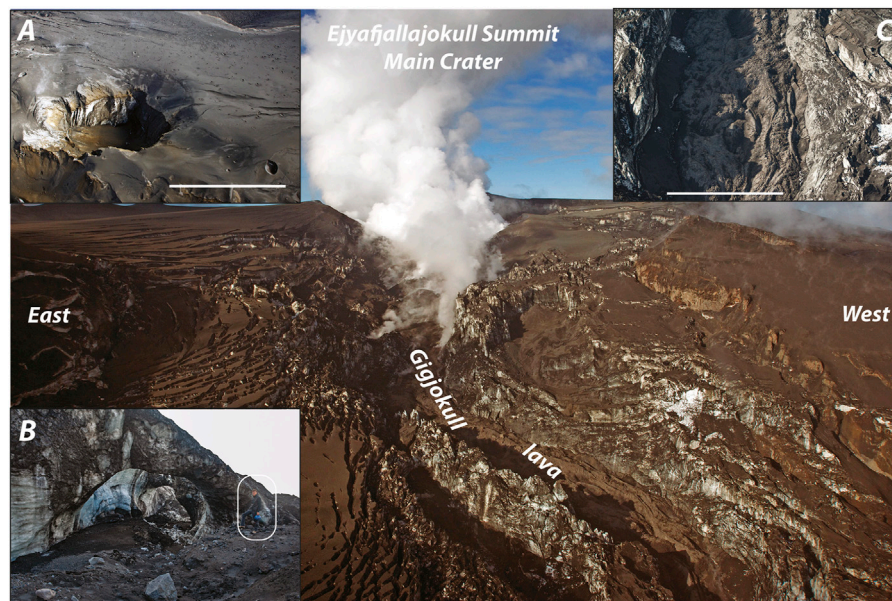
FIGURE 5 | Effects of ice on the 2010 Eyjafjallajökull eruption, south-central Iceland. Main view is from the north looking at the tephra-covered ice of Gigjökull and the summit of Eyjafjallajökull, with the canyon formed by meltwater and lava in the middle of the image. **(A)** An explosion crater in the summit ice partly filled with tephra. **(B)** An ice 'arch' remnant of an N-channel at the base of Gigjökull through which lava migrated beneath the ice. **(C)** The last stage of lava effusion was a subaerial, blocky lava emplaced into an ice canyon that confined the lava.

Longer-lived volcanoes have the capacity to span glacial-interglacial transitions such that only select morphological elements serve to record cryogenic periods of eruption (**Figures 4E–G**). At Hoodoo Mountain, a volcano in northwestern British Columbia that had eruptions spanning 100 k.y. (Edwards et al., 2002), the prominent cliffs that circumscribe much of the base of the edifice as well as its broad, gently rounded summit that still hosts a small ice-cap form a distinct, squat morphology (**Figure 4E**). Mount Rainier is a Cascade volcano with a morphology that is typical of andesitic stratovolcanos, however, its extended (500 k.y.) eruption history includes periods of ice-confined volcanic eruption which have not created obvious morphological elements reflecting its glaciovolcanic history (**Figure 4F**; Sisson et al., 2014). Detailed work by Lescinsky and Fink (2000), however, identified a number of lava ridges which they established as resulting from lateral impoundment by bounding glaciers. At more mafic long-lived volcanoes like Villarrica and Osorno, in central Chile, fluid lavas largely obscure the morphological influences of the cryogenic environment, where young volcanic cones and lavas are likely built upon older, glaciovolcanic deposits (**Figure 4G**).

CRYOSPHERIC IMPACTS ON VOLCANIC ERUPTIONS

The complex (**Figure 5**) influences of the cryospheric environment on volcanic eruptions has been well documented during several historic eruptions (e.g., 1980 Mount St. Helens, 1996 Gjálp, 2004 Grimsvötn, 2009 Redoubt, 2010 Eyjafjallajökull, 2012–13 Tolbachik; cf. Smellie and Edwards, 2016). Syn-eruption melting of the enclosing ice leads to dynamic pressure changes at the vent and in the environment as coherent icesheet transitions to fracturing and collapsing of the icesheet, and to a rising and falling column of meltwater. Observations on modern eruptions in the cryospheric environment show that the ice melting and formation of ephemeral englacial lakes can be rapid but are areally-limited so that volcanic deposits are largely confined by the enclosing ice (e.g., Jude-Eton et al., 2012; Magnusson et al., 2012; Oddsson, 2016). The linked 2010 Eyjafjallajökull and Fimmvörðuhals eruptions in Iceland are a clear example of this complexity during an essentially single, continuous volcano-magmatic event within the cryosphere (**Figure 5**).

The initial flank eruption of basalt at Fimmvörðuhals from mid-March to mid-April produced lavas that flowed across the top of a 3–5 m snowpack but eventually melted through snowpack to produce ice-confined lavas (Edwards et al., 2012). Locally however, a combination of thicker basal lava breccia and thicker snowpack resulted in several lavas crossing and remaining on top of the snow, even months after the eruption stopped. Just 1 day after the initial eruption ended on 13 April, the eruption shifted to the volcano summit and vented through the ~200 m thick summit glacier and produced at least three explosive craters (Magnusson et al., 2012; **Figure 5B**). One of these eventually enlarged to become the main vent for the eruption and was partly filled with scoria and course tephra. These initial explosive eruptions produced jökulhlaups that predominately passed
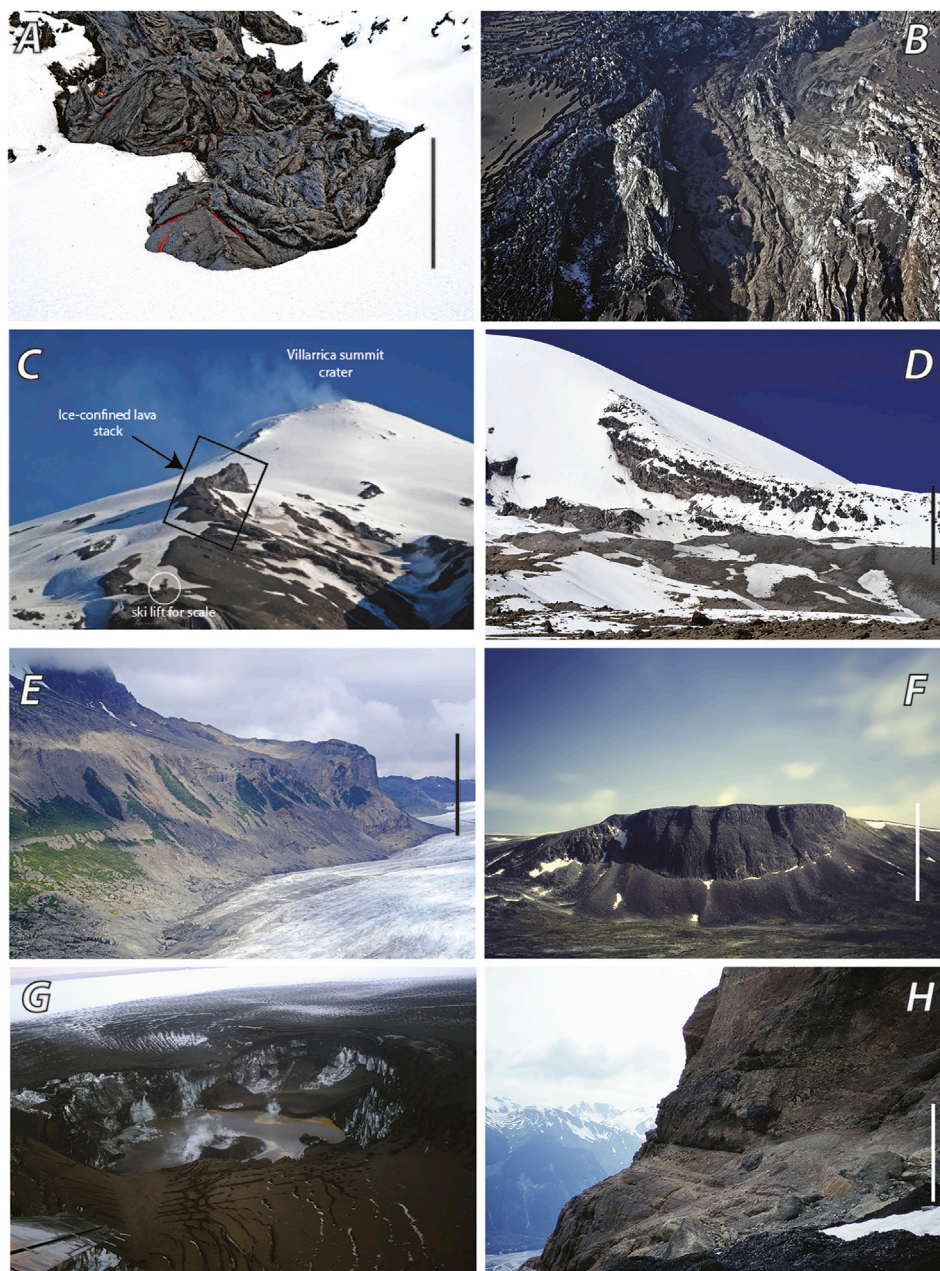
FIGURE 6 | Glaciovolcanic deposits whose structure and character are indicative of emplacement in a cryospheric environment. **(A)** Lava flow emplaced onto of snowpack, which subsequently melted through the snow, Tolbachik, Russia. **(B)** Lava confined within a canyon of ice, Gigjökull, Iceland. **(C)** Stacked lava ridge on the north summit of Villarrica volcano, Chile. **(D)** Stacked lava ridge on the western summit dome, Coropuna volcano, Peru. **(E)** Ice-bounded lava on the northeastern side of Hoodoo Mountain volcano, British Columbia, Canada. **(F)** Ice dammed lava at Llangorse Mountain, northern British Columbia, Canada. **(G)** Eruption site from 2004 Grimsvötn, Iceland, showing tephra covered glacier, englacial lake, and newly produced tephra cone. **(H)** Horizontally-bedded volcaniclastic deposits at 1500 m a.s.l. on the southern flank of Hoodoo Mountain volcano, British Columbia, Canada.

down the north side of the volcano, through Gigjökull, which is the largest outlet glacier on the north side of Eyjafjallajökull. These initial floods likely exploited and enlarged the pre-existing subglacial drainage N- and R-channels. Between 18 April and 4 May, continued summit explosive eruptions were accompanied by lava effusion. The lavas initially flowed beneath the surface of

Gigjökull, exploiting the same R- and N-channels that had been enlarged by meltwater (Oddsson et al., 2016; **Figure 5C**). Later "subaerial" lava flowed down a narrow, ice-confined channel through Gigjökull (**Figure 5D**). Distinctive textures of the lava emplaced beneath the ice, including thick outer vitric rinds and highly fractured surfaces, are interpreted to be indicative of an

external "coolant" (Oddsson et al., 2016). This single event produced: 1) proximal and distal tephra airfall deposited on land, neighbouring glaciers, and in the ocean, 2) tephra syn-eruptively entrained and transported by meltwater flowing beneath Gigjökull glacier and by the Markarflöt River, 3) lava emplaced on top of snowpack, 4) lava emplaced within tunnels at the base of Gigjökull, and 5) lava emplaced subaerially within an ice canyon.

Outstanding questions concern how the cryospheric environment impacts magma fragmentation and explosivity. Recent work on eruptions in aqueous (englacial) environments by Rowell et al. (2021) suggests that magma-water interactions can produce more energetic eruption columns. As discussed above, the presence of ice and water can increase rates of heat transfer from the magma (and its fragments) to its environment. The accelerated cooling causes rapid increases in melt viscosity to the point of the glass transition temperature where brittle behaviour dominates over ductile. The thermal stresses within volcanic glass raised by rapid heat extraction provides a means for efficient particle fragmentation. Liquid water trapped within low permeability deposits at high-temperature is easily vaporized causing explosive fragmentation driven by expansion of the gas phase (e.g., Dürig et al., 2020).

CRYOSPHERIC IMPACTS ON VOLCANIC LITHOFACIES

The cryospheric (**Figure 6**) eruption environment exerts a pronounced control on the properties, geometries and distributions of volcanic lithofacies. Salient summaries and descriptions of characteristic glaciovolcanic lithofacies are provided by Smellie (2000), Edwards et al. (2014), Russell et al. (2014), and Smellie and Edwards (2016), as well as, in many deposit-specific studies. Here we limit our discussion to the main elements that are diagnostic of eruptions in the cryosphere (**Figure 6**). These features include anomalous deposit morphologies and properties that reflect confinement, anomalous high rates of cooling (i.e. quenching), and, especially, the presence of a standing body of meltwater in a physiographically implausible location. Most of these deposits show evidence for complicated cooling histories involving variable rates and directions of heat transfer.

Evidence for confinement of the distributions of lavas and volcaniclastic deposits is the signatory of the cryospheric eruption environment. This impoundment can be recorded by deposit geometry, distribution, and other properties. While snow and ice can temporarily support the mass of an overlying lava (**Figure 6A**), heat transfer from the base of the lava eventually leads to the lavas sinking into the cryospheric cover (**Figure 6B**). This has been well documented at historic eruptions in Iceland (Edwards et al., 2012) and in Russia (Edwards et al., 2015). Horizontal to shallowly-dipping sequences of lava perched near the summits of stratovolcanoes have been uniquely interpreted as resulting from ice confinement (Lescinsky and Fink, 2000; **Figures 6C,D**). Impoundment or confinement commonly results in overthickened lavas, which is especially

evident for low viscosity lava (i.e., phonolite, basalt, nephelinite, basanite; Harder and Russell, 2007; **Figures 6E,F**) but also found in intermediate composition glaciovolcanic lavas. The extreme case of ice-confined effusive volcanism leads to the formation of lava-dominated tuyas (Kelmen et al., 2002; Wilson et al., 2019; Hodgetts et al., 2021). The key to interpreting these features as having formed in a cryospheric environment depends on there being no logical present-day physiographic explanation for confinement of the flow of lavas.

On a per volume basis most silicate melts release enough heat through cooling to melt about 3–10 times an equivalent volume of ice. Regardless, ice can effectively impede the flow of lava for two main reasons. Firstly, the continuous unimpeded flow of lava would require the volumetric rate of ice melting to match the eruptive flux. Although the heat content of lava is more than sufficient to melt the ice, the time scales of heat transfer from lava to ice are too slow relative to most effusive fluxes. Edwards et al. (2012) showed that lavas can flow onto and across the top of snow or ice with little melting for all but the very slowest-moving flows. This has also been demonstrated experimentally (Edwards et al., 2013), and observed at a number of eruptions (e.g., 1947 Hekla, Einarson, 1949; 2010 Fimmvörðuhals, Edwards et al., 2012; Edwards et al., 2013 Tolbachik, Edwards et al., 2015). Secondly, cooling the fronts and sides of advancing lava causes a reduction in temperature and a marked increase in viscosity causing a decrease in velocity and thickening of the lava front. The cooler lava is an insulator preventing efficient heat transfer from the hot lava interior to ice (Wilson and Russell, 2020). The main difficulty in using "overthickened" lavas as indicators of ice-confinement is that we lack coherent global databases that document the range of thicknesses for lavas associated with subaerial eruption environments.

Volcaniclastic deposits can also show the effects of confinement by their geometry and distributions and, thus, can also be indicative of cryospheric environments. The main features that are likely to be preserved from volcaniclastic/pyroclastic deposits are found proximally. More distal or dispersed deposits that populate the ice surface at the time of eruption are likely to be lost, or to be transported within ice from the eruption site. Deposits that accumulate within the cauldron overlying the vent will have limited distributions (<1 km; **Figure 6G**); they may have subhorizontal bedding even when present topography is steeply sloped (**Figure 6H**) or presumably over-steepened bedding if deposited abutting an ice wall. Either way, the preserved deposits will have geometries that show little thinning with distance from the vent and terminate with anomalous thicknesses and/or geometries (e.g., Smellie, 2000).

Polygonal/columnar jointing is an important volcanological feature that occurs in a wide variety of deposits (e.g., lavas, dykes, and ignimbrites) and provides a record of paleo-cooling history (e.g., Long and Wood, 1986; Goehring and Morris, 2008; **Figure 7**). Cooling-induced joints inform on the transient rates and directions of heat flow; column diameter is inversely proportional to cooling rate and the column orientation (length) indicates heat flow direction.
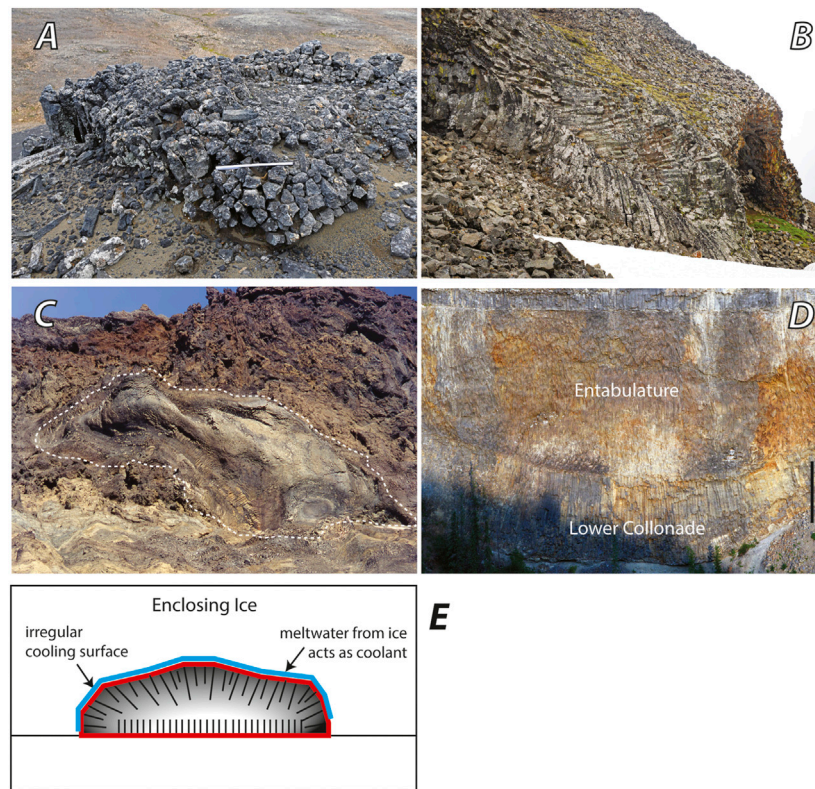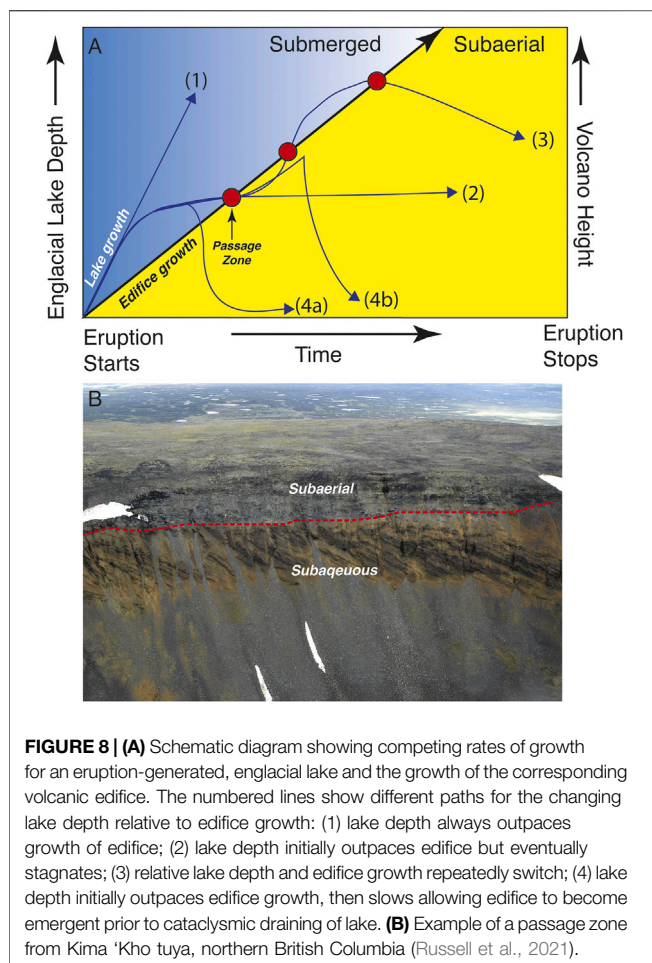
FIGURE 7 | Polygonal jointing examples from glaciovolcanic deposits. **(A)** Anomalously small columnar joints in basaltic lava at Breidravirki tindar, Iceland. **(B)** Highly-jointed mass of trachyte within breccia carapace at Hoodoo Mountain volcano, British Columbia. Jointing is vertical at the contacts between lava and breccia, but is rotated through 90 degrees such that it is horizontal in the middle. **(C)** Radiating joints in ice-confined lava from Mathews Tuya, British Columbia. **(D)** An example of typical polygonal jointing in a subaerial lava from northern British Columbia, with vertical joints in the basal colonnade and irregular joint orientations in the overlying entabulature. **(E)** Schematic drawing illustrating joint orientations in a lava emplaced into ice.

In subaerial environments, cooling columns are commonly well-organized into a lower and upper colonade that are oriented perpendicular to cooling surfaces (i.e., ground, valley walls, and etc.). The colonnades are sometimes separated by an entabulature comprising subvertically-oriented columns with a limited range in sizes (**Figure 7D**). In cryogenic environments, columnar jointing is much more varied and, in many cases, can be diagnostic, or provide supporting evidence, of that environment (e.g., Lescinsky and Fink, 2000; Edwards and Russell, 2002; Lodge and Lescinsky, 2009; Forbes et al., 2014). Lavas cooled in glaciovolcanic settings commonly feature fine-scale columns (cube shaped or small diameter columns; **Figure 7A**) that are indicative of rapid cooling. Column orientations are also commonly diagnostic. In many glaciovolcanic deposits the axes of columns populating the cliff faces of lavas are subhorizontal indicating efficient and sustained heat transfer outwards to a surface that is no longer there (**Figure 7B**). Given the settings and geography of these deposits, at relatively high elevations and/or latitudes, the obvious candidate for the missing confining material is a mass of ice, which explains the anomalous thickness of lava and orientations of columnar joints. In other situations, glaciovolcanic lava masses have radiating and curving clusters of columnar joints (i.e., lobes or channels; **Figure 7C**). Commonly the columns also show a well-organized gradual

increase in diameter moving from the exterior surface inwards. The size gradation is a record of relative rates of heat transfer at the moment of columnar joint propagation and shows that heat loss is most efficient on the exterior surface and significantly slower in the interior of the lava mass. The radiating cluster of columns indicates that the exterior surface lava mass was cooling rapidly in all directions and heat was transferred efficiently to an enveloping medium (**Figure 7E**). The sometimes observed inward-curving character of the columns shows how the heat transfer direction changed as the columns propagated inwards from the exterior surface.

Eruptions within ice sheets lead to rapid melting and collapse of the overlying ice and commonly produce an englacial lake whose depth is dictated by the amount and rate of melting, the flux of volcanic material, the rate of sub-ice leakage, and the thickness of the confining ice (e.g., Russell et al., 2021). Eruptions into a standing body of water result in distinctive volcanic lithofacies that can be diagnostic, while not definitive, of the cryospheric environment including: pillow lava, pillow-lava breccias, hyaloclastite, peperitic dykes, lava-fed deltas, and pervasive and variable palagonitization of the deposits (cf. Smellie and Edwards 2016 for summaries and references). Pervasive palagonitization requires abundant vitric material, water and heat. Melting of enclosing ice produces abundant

FIGURE 8 | (A) Schematic diagram showing competing rates of growth for an eruption-generated, englacial lake and the growth of the corresponding volcanic edifice. The numbered lines show different paths for the changing lake depth relative to edifice growth: (1) lake depth always outpaces growth of edifice; (2) lake depth initially outpaces edifice but eventually stagnates; (3) relative lake depth and edifice growth repeatedly switch; (4) lake depth initially outpaces edifice growth, then slows allowing edifice to become emergent prior to cataclysmic draining of lake. **(B)** Example of a passage zone from Kima 'Kho tuya, northern British Columbia (Russell et al., 2021).

heated water, and, because the deposits are largely confined to the vent area by enclosing ice, cooling is less efficient. Additionally, dykes are commonly found within palagonitized glaciovolcanic deposits, and their emplacement into the tephra is another source of heat as the dykes cool and solidify, helping to maintain higher temperatures within the tephra pile (e.g., Edwards et al., 2009; Harris Russell, 2022).

Taken individually, most of these lithofacies are not exclusively diagnostic of glaciovolcanism but they clearly demand an aquatic environment and are strong evidence for a standing body of water. The key, as seen at many tuyas, is having multiple lines of evidence for a substantial (deep) standing body of water in situations where there is clearly no obvious means to create and sustain such a lake. Collectively these observations provide the evidence for a cryospheric eruption environment (e.g., Smellie and Edwards, 2016; Smellie, 2018).

DISCUSSION

When compared to subaerial and subaqueous environments, the cryospheric environment is the most dynamic and complex. This is well-illustrated in two examples. Firstly, by an examination of

the stability and dynamics of syn-eruptive englacial lakes of melt water formed during glaciovolcanic eruptions (cf. Smellie and Edwards, 2016; Russell et al., 2021). Secondly, by an analysis of how changes in pressure during eruptions can impact vesiculation and vesiculation induced fragmentation.

Dynamic Self-Regulation of Englacial Lakes

The englacial lakes produced during glaciovolcanic eruptions are ephemeral—they rise in depth as they fill with meltwater but are regulated by background leakage via sub-ice drainages systems or susceptible to catastrophical drainage events when water pressures exceed the ice load pressure. Additionally, as englacial lakes form and grow during an eruption they are filling not only with meltwater, but also with a rapidly aggrading volcanic edifice. The competition between inputs of water and volcanic materials can produce a range of conditions that have different consequences for both (**Figure 8A**). For example, some glaciovolcanic pillow ridges (also referred to as "tindar"; see **Figure 4C**) in Iceland and in British Columbia formed during eruptions where the increase in edifice height was much slower than the rise in the enclosing englacial lake such that the edifice was totally emplaced subaqueously (e.g., Pollock et al., 2014; Edwards et al., 2009; **Figure 8A** path 1). A second, relatively common scenario is expressed by the iconic, flat-topped tuya volcanoes that have been studied in detail in Iceland (see **Figure 4A**; e.g., Jones, 1969; Skilling, 2009; Pedersen and Grosse, 2014), British Columbia (Mathews, 1947; Hickson,2000; Moore, 1970; Edwards et al., 2012), and the Antarctic (Smellie, 2009). During these eruptions, the lake surface elevation remains higher than the growing edifice, producing subaqueous facies deposits, until at some point where the edifice becomes emergent and commonly creating a cap of horizontal subaerial lavas (**Figure 8A** path 2). The stratigraphic surface produced when the edifice breaches the lake surface is referred to as a "passage zone" (Jones, 1969). Locally, the competition between water and volcanic materials is clearly demarcated by passage zones (**Figure 8B**). Passage zones are diachronous, stratigraphically-defined surfaces that record subaqueous-subaerial transitions during volcanic eruptions that start subaqueously but later transition to subaerial conditions (e.g., Fuller, 1931; Werner and Schmincke, 1999; Nelson, 1975; Smellie, 2009; Mathews, 1947; Jones, 1969; Smellie and Edwards, 2016; Russell et al., 2021). In the cryospheric environment, passage zone surfaces provide records of the heights and depths of syn-eruptive englacial lakes of meltwater at a specific point in time and space (see detailed review and references in Russell et al., 2021). Thus, they also help document the presence and nature, including minimum thickness, of the enclosing ice sheet. All passage zones are diachronous and, thus, document dynamic changes in lake levels through time (Smellie, 2000; Russell et al., 2014). For example, gradients in passage zone elevations record the rates of rise and fall in englacial lake levels relative to the rates of edifice growth (Russell et al., 2014; **Figure 8A**). Volcanoes having similar morphological features have long been postulated to occur on Mars (Allen, 1979).
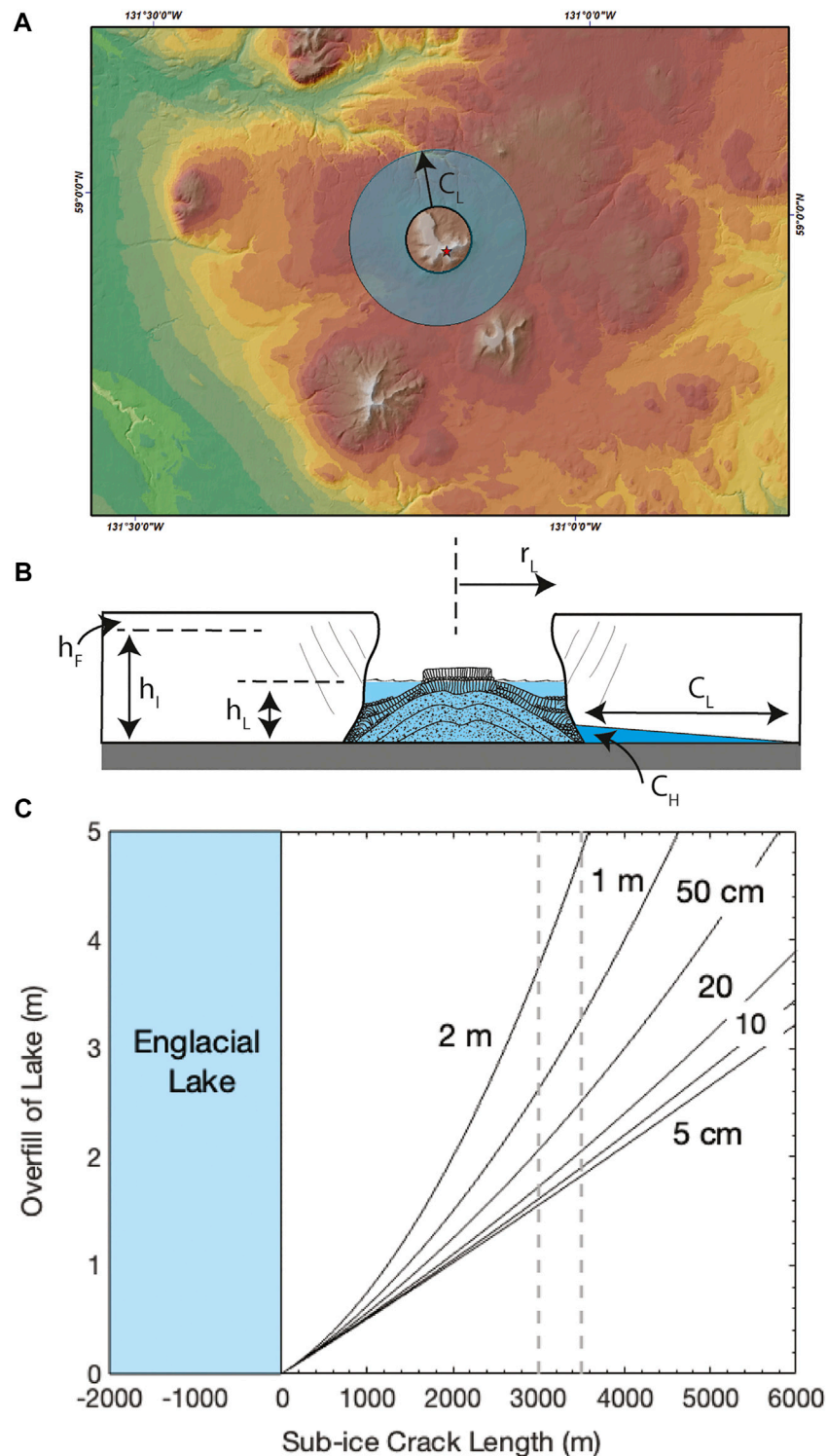
FIGURE 9 | Model for growth and radial propagation of sub-ice crack linked to major drainage systems driven by overfilling of syn-eruptive englacial lake. **(A)** Geometric sketch of model for predicting length (*CL*) of sub-ice wedge-shaped cracks as a function of ice and lake dimensions. **(B)** Model values of crack length versus overfill of lake above an equilibrium depth and contoured for the maximum opening of the crack near the englacial lake. **(C)** The major drainages on the Kawdy plateau surrounding the Kima Kho volcano are less than 3–3.5 km from the vent. The model curves show that very slight rises in lake level would be capable of supporting opening and propagation of sub-ice cracks that intersect those drainages. Conservative initial crack openings of 10–20 cm would find such drainages with only a 1–2 m rise in lake level over its equilibrium height.

In a few cases, the competition between edifice growth and lake deepening is complex, and multiple passages zones can form (**Figure 8A** path 3; e.g., Smellie, 2009; Skilling, 2009; Russell et al., 2014, Russell et al., 2021). A final general path that is less frequently identified is one where, at some point in the eruption, the lake drains catastrophically, which is referred to as a "jökulhlaup." These sudden drainage events are well documented during eruptions at Grimsvötn in Iceland, although not all jökulhlaups originate during or because of volcanic activity (Gudmundsson et al., 2008). Syn-eruptive jökulhlaups have been postulated at volcanoes that were still subaqueous when the drainage event happened (**Figure 8A** path 4a; Hoskuldsson et al., 2006; Owen et al., 2012), as well as for subaerial ones (**Figure 8A** path 4b; Russell et al., 2021).

Russell et al. (2021) recently described a sequence of passage zones within a single glaciovolcanic edifice thereby providing a temporal (relative) record of changes in the depth and volume of the ice-impounded lake during the eruption. Kima' Kho tuya is a highly dissected, large volume (~3.5 km^3; 3 times the volume of Surtsey) basaltic glaciovolcano situated in northwestern British Columbia and covering an area of ~21.0 km^2 (**Figure 9A**). The edifice has a maximum elevation of ~1,957 m above sea level (masl) and a relief of ~490 m above the Kawdy Plateau (~1,460 ± 20 masl). The distribution of volcanic lithofacies indicate that the volcano was enclosed by a >400 m thick glacier and erupted into an ice-confined (englacial) lake having a radius of ~2. The three passage zones (Pz$_{1-3}$) record the transient levels (i.e. elevation) of the englacial lake caused by syn-eruptive melting of the enclosing ice sheet and subsequent leakage and drainage.

We assume that progressive melting of the enclosing ice sheet resulted in a cylindrical cauldron. The initial (and maximum) lake level attending the explosive phase of eruption is marked by a passage zone situated at 1,800 masl indicating a englacial lake depth of ~340 m. The lake stored a peak water volume of ~2.3 km^3, which also accounts for the submerged volume of the tephra cone (~2.0 km^3). The passage zone is horizontal and extends over 1–2 km (see **Figure 8B**) suggesting a long-lived, stable configuration where lake volume and height were maintained as the eruption transitioned from explosive to effusive. This implies that the increase in water by melting or increase in lake volume by edifice displacement, is balanced by the ambient rates of subglacial drainage for an extended period. Drainage beneath the ice during the initial phase of the eruption must have been limited to allow for storage of meltwater and growth of the englacial lake. However, the fact that the lake level did not rise above 1,800 masl, despite >2 km^3 of surplus meltwater (i.e. over the ~2.3 km^3 stored in the lake), implies a leaky englacial lake system (Russell et al., 2014).

Kima 'Kho tuya formed within the Cordilleran ice sheet at about 1.9 Ma (Edwards et al., 2020; Russell et al., 2021). Ice sheets commonly feature 10s of metres of firn at their surface (Cuffey and Paterson, 2010), which is a more permeable than compacted snow pack but much less so than glacial ice (h_I). In certain situations, firn offers a means of supraglacial draining of meltwater that can modulate englacial lake depth (e.g., Smellie, 2018). However, ice sheets over a certain total thickness (h_T) will never have lake levels high enough to intersect the firn. The maximum volume of meltwater available for the englacial lake (V_L) assuming no loss by subglacial leakage is:

$$V_L = 0.9 \, \pi \, (h_I + h_F) \, r_L^2$$

Drainage through the firn requires:

$$V_L \geq \pi \, (h_T - h_F) \, r_L^2$$

implying that supraglacial drainage through the firn can only occur where:

$$h_F \geq 0.1 \, h_T$$

Firn thickness (h_F) can vary from 40–120 m in which case firn drainage is limited to ice sheets that have total thicknesses ($h_T = h_I + h_F$) less than 400–1,200 m, and where all of the melt water produced in the eruption is stored and not lost to leakage or syn-eruption evaporation.

One explanation for the apparent long-lived, stable configuration of the initial englacial lake at Kima 'Kho tuya is that, at an elevation of 1,800 masl, the lake depth of 340 m was in hydraulic balance with the ice sheet. Subglacial drainage of meltwater was minimal and controlled by the permeability of the enclosing ice and the nature of the basal interface between the ice sheet and its substrate. In this situation, the water column within the englacial lake exerts pressure at the base of the ice sheet that is less than or equal to the overlying load of the ice.
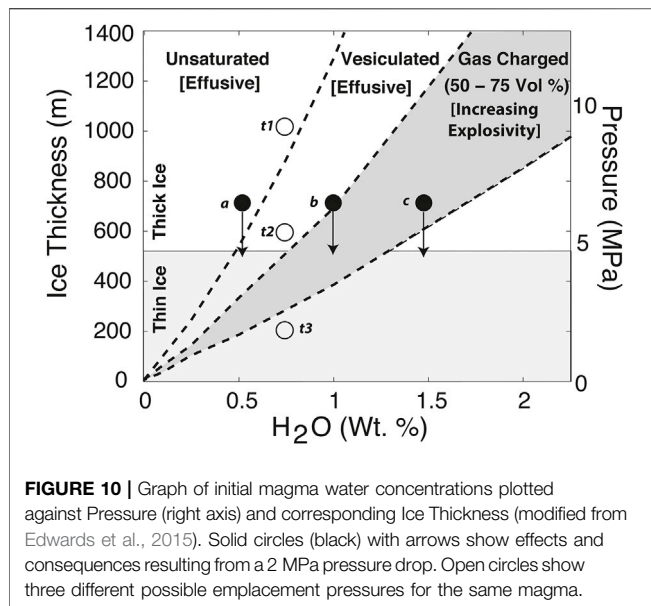
Evidence presented by Russell and Edwards. (2021) is consistent with a cataclysmic drainage event for the initial englacial lake formed during the eruption. At this tuya the lake refilled and produced two later passage zones, which raises the question of what triggered the jökulhaup. Water pressure in the lake has the capacity to lift the base of the enclosing ice wall and fill any cracks or fissures localized at the basal contact between the ice sheet and its substrate. If the system was near equilibrium or the hydraulic pressure was slightly in excess of the glaciostat, small excursions in lake level could trigger major drainage events. These jökulhaups would be catalyzed by propagation of sub-ice, water-filled cracks that intersect major pre-existing sub-glacial drainage systems. The additional head from "overfilling" of the lake (i.e. > 1,800 masl) needed to support filling of sub-ice cracks that could find and exploit pre-existing major drainages proximal to the Kima Kho volcano (**Figure 9A**) can be estimated by considering a right-angled radial wedge-shaped crack as illustrated (**Figure 9B**) with a total volume (V_c) of:

$$V_c = \frac{1}{2} \pi \, C_H \left[C_L^2 + 2 \, C_L \, r_L \right]$$

where r_L is the radius of the englacial lake, C_H is the maximum opening of the crack (near the vent), and C_L is the length of the 3-D crack body. The additional volume added to the lake (V_L) that provides the additional head for filling the crack is:

$$V_L = \pi \, \Delta_L r_L^2$$

where Δ_L is the rise in lake level (m). The balance between overfilling of the lake and filling the crack therefore is:

FIGURE 10 | Graph of initial magma water concentrations plotted against Pressure (right axis) and corresponding Ice Thickness (modified from Edwards et al., 2015). Solid circles (black) with arrows show effects and consequences resulting from a 2 MPa pressure drop. Open circles show three different possible emplacement pressures for the same magma.

$$V_L > V_c$$

and as an equality:

$$\pi \, \Delta_L \, r_L^2 = \frac{1}{2} \pi \, C_H \left[C_L^2 + 2 \, C_L \, r_L \right]$$

Values of C_L can be solved for from the quadratic expression:

$$C_L^2 + 2 \frac{r_l}{C_H} C_L + \frac{2 \, \Delta_L \, r_L^2}{C_H} = 0$$

which depends on the radius of the englacial lake, the rise in stable lake level, and the initial crack thickness (**Figure 9B**).

This simplified analysis shows that, at least in the landscape near Kima 'Kho tuya, only small volumes of the englacial lake water are needed to produce and fill crack openings (0.1 cm–1 m; **Figure 9C**) that could "find" pre-existing drainage networks (minimum of 3 km at Kima 'Kho; **Figure 9A**), thereby preventing lake overfilling and potentially triggering jökulhaups. This crack propagation process can enable englacial lakes to remain in dynamic equilibrium with their enclosing ice, leading to lake level fluctuations only found in the cryospheric eruption environment.

Dynamic Transitions in Vesiculation and Fragmentation

As illustrated above, the cryospheric eruption environment can produce repeated changes, slow or rapid, in vent conditions due to differences in englacial lake water levels. These changes can also change the state of vesiculation in a magma and lead to shifts from effusive to explosive activity. As for all volcanic eruptions, one of the main controls on explosivity during glaciovolcanic eruptions is the relationship between external pressure and the magma's volatile solubility (**Figure 10**; Owen et al., 2012; Edwards et al., 2014). In general, high glaciostatic/hydrostatic pressures (i.e. thick ice) and

"dry" magmas favor effusive eruptions, while lower pressures (i.e. thin ice) and "wet" magmas favor explosive eruptions. Thus, even some "thick" ice eruptions may initially be explosive, which favors high heat transfer efficiencies, rapid melting, and more dangerous jökulhaups (Gumundsson, 2003). During glaciovolcanic eruptions, the effective pressure is complicated by the nature of the ice "overburden," which melts and fractures as the eruption proceeds. The presence of meltwater also affects eruption style by promoting "quench" fragmentation during effusive eruption, as well as phreatomagmatic explosivity driven by shockwave breakup of the magma followed due to rapid expansion of trapped liquid water being converted to steam. The relative importance of quench, phreatomagmatic, and magmatic fragmentation will ultimately depend on the unique magmatic and glacial conditions for any given eruption, but during eruptions in the cryospheric environment as they be produced repeatedly, leading to complex stratigraphies and grain componentry (e.g., Schopka et al., 2006; Jude-Eton et al., 2012).

Two different aspects of the cryospheric environment have important controls on the state of vesiculation, hence, eruption styles and properties of tephra. Firstly, the waxing and waning of continental ice sheets has occurred over varying time-scales during the Pleistocene (Cuffey and Paterson, 2010). The pre-1 Ma cycles spanned approximately 40 ky, and the more recent post-1 Ma cycles span about 100 ky. These time-scales are shorter than the lifespan of polygenetic glaciovolcanoes (e.g., Hoodoo Mountain; many stratovolcanoes), which means that repeated eruptions from the same edifice will likely not always occur under the same glaciostatic pressures. So, even if the source magmas remain relatively constant in composition with respect to dissolved volatiles, eruptions under different ice conditions will produce deposits with different vesicularities and also potentially different eruption styles. For example, for a magmatic system with 0.75 weight percent dissolved H_2O, a cryospheric eruption during a glacial maxima (~1,000 m of ice) might be effusive (t1, **Figure 10**), while the same eruption during different stages of ice thickening or thinning could be effusive but with a vesiculated magma (t2, **Figure 10**) or explosive (t3, **Figure 10**). Secondly, rapid changes in pressure such as those seen periodically by drainage of englacial lakes in Iceland (e.g., Grimsvötn) are more than sufficient to drive magmatic systems into different eruption states. Given three different magmas each with different concentrations of dissolved H_2O (**Figure 10**, points a, b, c), a 2 MPa drop in pressure due to catastrophic lake drainage can change the magma state from effusive undersaturated to saturated and vesicular (**Figure 10** point a), from effusive vesiculated to highly vesiculated (**Figure 10** point b), or from effusive vesiculated to explosive (**Figure 10** point c).

SUMMARY

Volcanic eruptions within cryospheric environments are controlled by all of the variables and conditions found in subaerial and subaqueous eruption environments save, perhaps, the conditions attending deeper submarine eruptions (Cas and Simmons, 2018). Vent systems can be repeatedly flooded by meltwater, and then drained. Initial stages of eruption are most influenced by environmental confinement but

sustained larger eruptions can evolve to support the more long-distance transport of tephra generally attributed to explosive subaerial eruptions (e.g., Eyjafjallajökull 2010). The unique characteristics of these deposits are key to recognizing their glaciovolcanic origins and provide the means to constrain the syn-eruptive cryospheric environmental conditions (e.g., depth of water, ice thickness). Given the wide-spread distribution of these deposits throughout the Plio-Pleistocene, they remain one of the largest land-based archives available for reconstructing past ice extents, thicknesses and hydrologies on Earth, as well as, other planetary bodies (Smellie and Edwards, 2016; Smellie, 2018; Edwards et al., 2020; Wilson and Russell, 2020). Because the it can change over relatively short time-scales, its englacial lakes can be highly dynamic, and eruptions within the it can transition to subaqueous and subaerial environments repeatedly, the cryospheric environment is the most complex eruption environment for volcano-magmatic systems.

AUTHOR CONTRIBUTIONS

BRE conceptualized the collaborative project. All three authors contributed figures, written text, ideas to the discussion, and participated in preparation of the final manuscript.

REFERENCES

Albino, F., Pinel, V., and Sigmundsson, F. (2010). Influence of Surface Load Variations on Eruption Likelihood: Application to Two Icelandic Subglacial Volcanoes, Grímsvötn and Katla. *Geophys. J. Int.* 181 (3), 1510–1524.

Andrew, R. E. B., and Gudmundsson, A. (2007). Distribution, Structure, and Formation of Holocene Lava Shields in Iceland. *J. Volcanol. Geotherm. Res.* 168, 137–154. doi:10.1016/j.volgeores.2007.08.01110.1016/j.jvolgeores.2007.08.011

Asmerom, Y., DuFrane, S. A., Mukasa, S. B., Cheng, H., and Edwards, R. L. (2005). Time Scale of Magma Differentiation in Arcs from Protactinium-Radium Isotopic Data. *Geology* 33 (8), 633–636. doi:10.1130/g21638ar.1

Belousov, A., Belousova, M., Edwards, B., Volynets, A., and Melnikov, D. (2015). Overview of the Precursors and Dynamics of the 2012-13 Basaltic Fissure Eruption of Tolbachik Volcano, Kamchatka, Russia. *J. Volcanol. Geotherm. Res.* 299, 19–20. doi:10.1016/j.jvolgeores.2015.04.009

Bindeman, I. N., Leonov, V. L., Izbekov, P. E., Ponomareva, V. V., Watts, K. E., Shipley, N. K., et al. (2010). Large-volume Silicic Volcanism in Kamchatka: Ar-Ar and U-Pb Ages, Isotopic, and Geochemical Characteristics of Major Pre-holocene Caldera-Forming Eruptions. *J. Volcanol. Geotherm. Res.* 189, 57–80. doi:10.1016/j.jvolgeores.2009.10.009

Capra, L., Roverato, M., Groppelli, G., Caballero, L., Sulpizio, R., and Norini, G. (2015). Glacier melting during lava dome growth at Nevado de Toluca volcano (Mexico): Evidences of a major threat before main eruptive phases at ice-caped volcanoes. *J. Volcanol. Geotherm. Res.* 294, 1–10. doi:10.1016/j.jvolgeores.2015.02.005

Capra, L. (2006). Abrupt Climatic Changes as Triggering Mechanisms of Massive Volcanic Collapses. *J. Volcanol. Geotherm. Res.* 155 (3), 329–333. doi:10.1016/j.jvolgeores.2006.04.009

Cas, R. A. F., and Simmons, J. M. (2018). Why Deep-Water Eruptions Are So Different from Subaerial Eruptions. *Front. Earth Sci.* 6. doi:10.3389/feart.2018.00198

Clague, J. J., and Ward, B. (2011). "Quaternary Glaciations–Extent and Chronology: A Closer Look," in *Chapter 44–Pleistocene Glaciation of British Columbia*. Editor J. Ehlers, P. L. Gibbard, and P. D. Hughes (United Kingdom: Elsevier, Developments in Quaternary Sciences Series) 15, 563–573. doi:10.1016/B978-0-444-53447-7.00044-1

Cuffey, K. M., and Paterson, W. S. B. (2010). *The Physics of Glaciers*. 4th Edition. U.S.A. Elsevier, 693p.

Curtis, A., and Kyle, P. (2017). Methods for Mapping and Monitoring Global Glaciovolcanism. *J. Volcanol. Geotherm. Res.* 333-334, 134–144. doi:10.1016/j.jvolgeores.2017.01.017

Dürig, T., White, J. D. L., Murch, A. P., Zimanowski, B., Büttner, R., Mele, D., et al. (2020). Deep-sea Eruptions Boosted by Induced Fuel-Coolant Explosions. *Nat. Geosci.* 13, 498–503.

Eason, D. E., Sinton, J. M., Grönvold, K., and Kurz, M. D. (2015). Effects of Deglaciation on the Petrology and Eruptive History of the Western Volcanic Zone, Iceland. *Bull. Volcanol.* 77, 47. doi:10.1007/s00445-015-0916-0

Edwards, B. R., and Russell, J. K. (2002). Glacial Influences on Morphology and Eruptive Products of Hoodoo Mountain Volcano, Canada. *Geol. Soc. Lond. Spec. Publ.* 202 (1), 179–194. doi:10.1144/gsl.sp.2002.202.01.09

Edwards, B., Russell, J., and Anderson, R. (2002). Subglacial, Phonolitic Volcanism at Hoodoo Mountain Volcano, Northern Canadian Cordillera. *Bull. Volcanol.* 64 (3), 254–272.

Edwards, B. R., Skilling, I. P., Cameron, B., Haynes, C., Lloyd, A., and Hungerford, J. H. D. (2009). Evolution of an Englacial Volcanic Ridge: Pillow Ridge Tindar, Mount Edziza Volcanic Complex, NCVP, British Columbia, Canada. *J. Volcanol. Geotherm. Res.* 185, 251–275. doi:10.1016/j.jvolgeores.2008.11.015

Edwards, B., Magnússon, E., Thordarson, T., Guðmundsson, M. T., Höskuldsson, A., Oddsson, B., et al. (2012). Interactions between Lava and Snow/ice during the 2010 Fimmvörðuháls Eruption, South-Central Iceland. *J. Geophys. Res.* 117, 21. doi:10.1029/2011JB008985

Edwards, B. R., Karson, J., Wysocki, R., Lev, E., Bindeman, I., and Kueppers, U. (2013). Insights on Lava–Ice/snow Interactions from Large-Scale Basaltic Melt Experiments. *Geology* 41 (9), 851–854. doi:10.1130/g34305.1

Edwards, B. R., Belousov, A., and Belousova, M. (2014). Propagation Style Controls Lava-Snow Interactions. *Nat. Commun.* 5, 5666. doi:10.1038/ncomms6666

Edwards, B., Kochtitzky, W., and Battersby, S. (2020). Global Mapping of Future Glaciovolcanism. *Glob. Planet. Change* 195, 103356. doi:10.1016/j.gloplacha.2020.103356

Einarsson, T. (1949). The Flowing Lava: Studies of its Main Physical and Chemical Characteristics. *Soc. Sci. Isl.* 4, 1–70.

Eksinchol, I., Rudge, J. F., and Maclennan, J. (2019). Rate of Melt Ascent beneath Iceland from the Magmatic Response to Deglaciation. *Geochem. Geophys. Geosyst.* 20 (6), 2585–2605. doi:10.1029/2019GC008222

Ferrier, K. L., Kirchner, J. W., and Finkel, R. C. (2007). "Erosion Rates Over Millennial and Decadal Timescales at Caspar Creek and Redwood Creek,

FUNDING

ACKNOWLEDGMENTS

Northern California," in *Proceedings of the Redwood Region Forest Science Symposium: What Does The Future Hold?*. Editor R. B. Standiford, G. A. Giusti, Y. Valachovic, W. J. Zielinski, and M. J. Furniss (Albany, CA: Pacific Southwest Research Station, Forest Service, U.S. Department of Agriculture), 357–358.

Forbes, A. E. S., Blake, S., and Tuffen, H. (2014). Entablature: Fracture Types and Mechanisms. *Bull. Volcanol.* 76. doi:10.1007/s00445-014-0820-z

Fuller, R. E. (1931). The Aqueous Chilling of Basaltic Lava on the Columbia River Plateau. *Amer. J. Sci.* 21, 281–300.

Gee, M. A., Taylor, R. N., Thirlwall, M. F., and Murton, B. J. (1998). Glacioisostacy Controls Chemical and Isotopic Characteristics of Tholeiites from the Reykjanes Peninsula, SW Iceland. *Earth Planet. Sci. Lett.* 164 (1), 1–5. doi:10.1016/s0012-821x(98)00246-5

Geyer, A., and Bindeman, I. (2011). Glacial Influence on Caldera-Forming Eruptions. *J. Volcanol. Geotherm. Res.* 202, 127–142. doi:10.1016/j.jvolgeores.2011.02.001

Glazner, A. F., Manley, C. R., Marron, J. S., and Rojstaczer, S. (1999). Fire or Ice: Anticorrelation of Volcanism and Glaciation in California over the Past 800,000 Years. *Geophys. Res. Lett.* 26 (12), 1759–1762. doi:10.1029/1999gl900333

Goehring, L., and Morris, S. W. (2008). Scaling of Columnar Joints in Basalt. *J. Geophys. Res.* 113, B10203. doi:10.1029/2007JB005018

Gowan, Evan J. (2019). Global Ice Sheet Reconstruction for the Past 80000 Years. *PANGAEA* 12, 1199. doi:10.1594/PANGAEA.905800

Gregg, T. K. P., and Fornari, D. J. (1997). Long Submarine Lava Flows: Observations and Results from Numerical Modeling. *J. Geophys. Res.* 103 (B11), 27517–27531. doi:10.1029/98JB02465

Gudmundsson, M. T., Larsen, G., Höskuldsson, A., and Gylfason, A. G. (2008). Volcanic Hazards in Iceland. *Jökull* 58, 251–268.

Gudmundsson, A. (1986). Mechanical Aspects of Postglacial Volcanism and Tectonics of the Reykjanes Peninsula, Southwest Iceland. *J. Geophys. Res.* 91 (B12), 12711–12721. doi:10.1029/jb091ib12p12711

Gudmundsson, M. T. (2003). in *Subaqueous Explosive Volcanism*. Editors J. D. L. White, J. L. Smellie, and D. A. Clague (United States: American Geophysical Union, Geophysical Monograph Series), 140, 61–72. doi:10.1029/140gm04*Melting of Ice by Magma-Ice-Water Interactions during Subglacial Eruptions as an Indicator of Heat Transfer in Subaqueous Eruptions*

Harðarson, B. S., and Fitton, J. G. (1991). Increased Mantle Melting beneath Snaefellsjökull Volcano during Late Pleistocene Deglaciation. *Nature* 353, 62–64.

Harder, M., and Russell, J. K. (2007). Basanite Glaciovolcanism at Llangorse Mountain, Northern British Columbia, Canada. *Bull. Volcanol.* 69 (3), 329–340. doi:10.1007/s00445-006-0078-1

Harris, M. A., Russell, J. K, Barendregt, J. K., R Porritt, L. A., and Wilson, A. (2022). Explosive Glaciovolcanism at Cracked Mountain Volcano, Garibaldi Volcanic Belt, Canada. *J. Volcanol. Geotherm. Res.* 423, 107477. ISSN 0377-0273. doi:10.1016/j.jvolgeores.2022.107477

Hickson, C. J. (2000). Physical Controls and Resulting Morphological Forms of Quaternary Ice-Contact Volcanoes in Western Canada. *Geomorphology* 32 (3-4), 239–261. doi:10.1016/s0169-555x(99)00099-9

Höskuldsson, A., Sparks, R. S. J., and Carroll, M. R. (2006). Constraints on the Dynamics of Subglacial Basalt Eruptions from Geological and Geochemical Observations at Kverkfjöll, NE Iceland. *Bull. Volcanol.* 68, 689–701.

Hodgetts, A. G. E., McGarvie, D., Tuffen, H., and Simmons, I. C. (2021). The Thórólfsfell Tuya, South Iceland - a New Type of Basaltic Glaciovolcano. *J. Volcanol. Geotherm. Res.* 411, 107175. doi:10.1016/j.jvolgeores.2021.10717510.1016/j.jvolgeores.2021.107175

Hooper, A., Ófeigsson, B., Sigmundsson, F., Lund, B., Geirsson, H., and Sturkell, E. (2011). Increased Capture of Magma in the Crust Promoted by Ice-Cap Retreat in Iceland. *Nat. Geosci.* 4 (11), 10–1038. doi:10.1038/ngeo1269

Hubbard, A., Sugden, D., Dugmore, A., Norddahl, H., and Pétursson, H. G. (2006). A Modelling Insight into the Icelandic Last Glacial Maximum Ice Sheet. *Quat. Sci. Rev.* 25, 2283–2296. doi:10.1016/j.quascirev.2006.04.001

Jellinek, A. M., and DePaolo, D. J. (2003). A Model for the Origin of Large Silicic Magma Chambers: Precursors of Caldera-Forming Eruptions. *Bull. Volcanol.* 65 (5), 363–381. doi:10.1007/s00445-003-0277-y

Jellinek, A. M., Manga, M., and Saar, M. O. (2004). Did Melting Glaciers Cause Volcanic Eruptions in Eastern California? Probing the Mechanics of Dike Formation. *J. Geophys. Res.* 109. doi:10.1029/2004JB002978

Jones, J. G. (1969). Intraglacial Volcanoes of the Laugarvatn Region, South-West Iceland-I. *Geol. Soc. London Quart. J.* 124, 197–211.

Jude-Eton, T. C., Thordarson, T., Gudmundsson, M. T., and Oddsson, B. (2012). Dynamics, Stratigraphy and Proximal Dispersal of Supraglacial Tephra during the Ice-Confined 2004 Eruption at Grímsvötn Volcano, Iceland. *Bull. Volcanol.* 74, 1057–1082. doi:10.1007/s00445-012-0583-3

Jull, M., and McKenzie, D. (1996). The Effect of Deglaciation on Mantle Melting beneath Iceland. *J. Geophys. Res. Solid Earth* 101 (B10), 2185–21828. doi:10.1029/96jb01308

Kelman, M. C., Russell, J. K., and Hickson, C. J. (2002) *Effusive Intermediate Glaciovolcanism in the Garibaldi Volcanic Belt, Southwestern British Columbia, Canada*. in *Special Publications*. Editors J. L. Smellie and M. G. Chapman (London: Geological Society, London, Special Publications), 202, 195–211. doi:10.1144/gsl.sp.2002.202.01.10

Kerr, F. (1948). *Lower Stikine and Western Iskut River Areas* 246, 94. Ottawa: Geological Survey of Canada Memoir; Canada Department of Mines.

Lambeck, K., Purcell, A., Funder, S., KJaeR, K. H., Larsen, E., and Moller, P. (2006). Constraints on the Late Saalian to Early Middle Weichselian Ice Sheet of Eurasia from Field Data and Rebound Modelling. *Boreas* 35, 539–575. doi:10.1080/03009480600781875

Lambeck, K., H., Rouby, A., Purcell, A., Sun, Y., and Sambridge, M. (2014). Sea Level and Global Ice Volumes from the Last Glacial Maximum to the Holocene. *PNAS* 111, 15296–15303. doi:10.1073/pnas.1411762111

Le Breton, E., Dauteuil, O., and Biessy, G. (2010). Post-glacial Rebound of Iceland during the Holocene. *J. Geol. Soc.* 167, 417–432. doi:10.1144/0016-76492008-126

Lescinsky, D. T., and Fink, J. H. (2000). Lava and Ice Interaction at Stratovolcanoes: Use of Characteristic Features to Determine Past Glacial Extents and Future Volcanic Hazards. *J. Geophys. Res.* 105 (B10), 23711–23726. doi:10.1029/2000jb900214

Lisiecki, L. E., and Raymo, M. E. (2005). A Pliocene-Pleistocene Stack of 57 Globally Distributed Benthic δ18O Records. *Paleoceanography* 20, 17. doi:10.1029/2004PA001071

Lodge, R. W. D., and Lescinsky, D. T. (2009). Fracture Patterns at Lava-Ice Contacts on Kokostick Butte, OR, and Mazama Ridge, Mount Rainier, WA: Implications for Flow Emplacement and Cooling Histories. *J. Volcanol. Geotherm. Res.* 185, 298–310. doi:10.1016/j.jvolgeores.2008.10.010

Long, P. E., and Wood, B. J. (1986). Structures, Textures, and Cooling Histories of Columbia River Basalt Flows. *Geol. Soc. Am. Bull.* 97, 1144–1155. doi:10.1130/0016-7606(1986)97<1144:stacho>2.0.co;2

Maclennan, J., Jull, M., McKenzie, D., Slater, L., and Grönvold, K. (2002). The Link between Volcanism and Deglaciation in Iceland. *Geochem.-Geophys.-Geosyst.* 3 (11), 1–25. doi:10.1029/2001gc000282

Magnússon, E., Gudmundsson, M. T., Roberts, M. J., Sigurðsson, G., Höskuldsson, F., and Oddsson, B. (2012). Ice-volcano Interactions during the 2010 Eyjafjallajökull Eruption, as Revealed by Airborne Imaging Radar. *J. Geophys. Res.* 117, 17. doi:10.1029/2012JB009250

Mathews, W. H. (1947). "Tuyas," Flat-Topped Volcanoes in Northern British Columbia. *Am. J. Sci.* 245 (9), 560–570. doi:10.2475/ajs.245.9.560

McDonough, W. F., and Sun, S.-S. (1995). The Composition of the Earth. *Chem. Geol.* 120 (3-4), 223–253. doi:10.1016/0009-2541(94)00140-4

McLeod, P., and Tait, S. (1999). The Growth of Dykes from Magma Chambers. *J. Volcanol. Geotherm. Res.* 92 (304), 231–245. doi:10.1016/s0377-0273(99)00053-0

Moore, J. G. (1970). Pillow Lava in a Historic Lava Flow from Hualalai Volcano, Hawaii. *J. Geol.* 78 (2), 239–243. doi:10.1086/627506

Nelson, P. H. H. (1975). The James Ross Island Volcanic Group of North-East Graham Land. *Sci. Rep. Br. Antarct. Surv.* 54, 1–64.

Owen, J., Tuffen, H., and McGarvie, D. W. (2012). Explosive Subglacial Rhyolitic Eruptions in Iceland Are Fuelled by High Magmatic H2O and Closed-System Degassing. *Geology* 41, 251–254. doi:10.1130/G33647.1

Peacock, M. A. (1926). The Vulcano-Glacial Palagonite Formation of Iceland. *Geol. Mag.* 63 (9), 385–399. doi:10.1017/s0016756800085137

Pedersen, G. B. M., and Grosse, P. (2014). Morphometry of Subaerial Shield Volcanoes and Glaciovolcanoes from Reykjanes Peninsula, Iceland: Effects of Eruption Environment. *J. Volcanol. Geotherm. Res.* 282, 115–133. doi:10.1016/j.jvolgeores.2014.06.008

Pedersen, G. B. M. (2016). Semi-automatic Classification of Glaciovolcanic Landforms: An Object-Based Mapping Approach Based on Geomorphometry. *J. Volcanol. Geotherm. Res.* doi:10.1016/j.jvolgeores.2015.12.015

Pliny the Younger (2014). *The Complete Works of Pliny the Younger*. Delphi Classics. Book 28.

Pollock, M., Edwards, B., Hauksdóttir, S., Alcorn, R., and Bowman, L. (2014). Geochemical and Lithostratigraphic Constraints on the Formation of Pillow-dominated Tindars from Undirhlíðar Quarry, Reykjanes Peninsula, Southwest Iceland. *Lithos.* 200, 317–333. doi:10.1016/j.lithos.2014.04.023

Praetorius, S., Mix, A., Jensen, B., Froese, D., Milne, G., Wolhowe, M., et al. (2016). Interaction between Climate, Volcanism, and Isostatic Rebound in Southeast Alaska during the Last Deglaciation. *Earth Planet. Sci. Lett.* 452, 79–89. doi:10.1016/j.epsl.2016.07.033

Rawson, H., Pyle, D. M., Mather, T. A., Smith, V. C., Fontijn, K., Lachowycz, S. M., et al. (2016). The Magmatic and Eruptive Response of Arc Volcanoes to Deglaciation: Insights from Southern Chile. *Geology* 44 (4), 251–254. doi:10.1130/g37504.1

Rowell, C. R., Jellinek, A. M., Hajimirza, S., and Aubry, T. J. (2021). External Surface Water Influence on Explosive Eruption Dynamics, with Implications for Stratospheric Sulfur Delivery and Volcano-Climate Feedback. *Volcanology.* doi:10.3389/feart.2022.788294

Russell, J. K., Edwards, B. R., Turnbull, M., and Porritt, L. A. (2021). Englacial Lake Dynamics within a Pleistocene Cordilleran Ice Sheet at Kima' Kho Tuya (British Columbia, Canada). *Quat. Sci. Rev.* 273, 107247. doi:10.1016/j.quascirev.2021.107247

Russell, J. K., Edwards, B. R., Porritt, L., and Ryane, C. (2014). Tuyas: a Descriptive Genetic Classification. *Quat. Sci. Rev.* 87, 70–81. doi:10.1016/j.quascirev.2014.01.001

Satow, C., Gudmundsson, A., Gertisser, R., Ramsey, C. B., Bazargan, M., Pyle, D., et al. (2021). Eruptive Activity of the Santorini Volcano Controlled by Sea-Level Rise and Fall. *Nat. Geosci.* 14, 586–592. doi:10.1038/s41561-021-00783-4

Schopka, H. H., Gudmundsson, M. T., and Tuffen, H. (2006). The Formation of Helgafell, Southwest Iceland, a Monogenetic Subglacial Hyaloclastite Ridge: Sedimentology, Hydrology and Volcano-Ice Interaction. *J. Volcanol. Geotherm. Res.* 152, 359–377. doi:10.1016/j.jvolgeores.2005.11.010

Sigvaldason, G. E., Annertz, K., and Nilsson, M. (1992). Effect of Glacier Loading/deloading on Volcanism: Postglacial Volcanic Production Rate of the Dyngjufjoll Area, Central Iceland. *Bull. Volcanol.* 54 (5), 385–392. doi:10.1007/bf00312320

Sims, K. W. W., Maclennan, J., Blichert-Toft, J., Mervine, E. M., Blusztajn, J., and Grönvold, K. (2013). Short Length Scale Mantle Heterogeneity beneath Iceland Probed by Glacial Modulation of Melting. *Earth Planet. Sci. Lett.* 379, 146–157. doi:10.1016/j.epsl.2013.07.027

Sinton, J., Grönvold, K., and Sæmundsson, K. (2005). Postglacial Eruptive History of the Western Volcanic Zone, Iceland. *Geochem. Geophys. Geosys.* 6, Q12009. doi:10.1029/2005GC001021

Sisson, T. W., Salters, V. J. M., and Larson, P. B. (2014). Petrogenesis of Mount Rainier Andesite: Magma Flux and Geologic Controls on the Contrasting Differentiation Styles at Stratovolcanoes of the Southern Washington Cascades. *Geol. Soc. Am. Bull.* 126 (1-2), 122–144. doi:10.1130/b30852.1

Skilling, I. P. (2009). Subglacial to Emergent Basaltic Volcanism at Hlodufell, South-West Iceland: A History of Ice-Confinement. *J. Volcanol. Geotherm. Res.* 185, 276–289.

Slater, L., Jull, M., McKenzie, D., and Grönvold, K. (1998). Deglaciation Effects on Mantle Melting under Iceland: Results from the Northern Volcanic Zone. *Earth Planet. Sci. Lett.* 164 (1), 151–164. doi:10.1016/s0012-821x(98)00200-3

Smellie, J. L., and Edwards, B. R. (2016). *Glaciovolcanism on Earth and Mars*. Cambridge, UK: Cambridge University Press.

Smellie, J. L. (2000). in *Encyclopedia of Volcanoes*. Editors Haraldur Sigurdsson, Bruce Houghton, Hazel Rymer, John Stix, and Steve McNutt (Amsterdam, Netherlands: Elsevier), 403–418.*Subglacial Eruptions*

Smellie, J. L. (2009) *Terrestrial Sub-ice Volcanism: Landform Morphology, Sequence Characteristics and Environmental Influences, and Implications for Candidate Mars Examples.* in *Preservation of Random Mega-Scale Events on Mars and Earth: Influence on Geologic History*. Editors M. G. Chapman and L. Leszthely (Geol. Soc. Am. Special Papers), 453, 55–76.

Smellie, J. L. (2018). in *Past Glacial Environments (Sediments, Forms and Techniques)*. Editors J. Menzies and J. J. M. van der Meer. 2nd edition (Amsterdam, Netherlands: Elsevier), 335–375. doi:10.1016/b978-0-08-100524-8.00010-5*Glaciovolcanism*

Sparks, R. S. J., and Cashman, K. V. (2017). Dynamic Magma Systems: Implications for Forecasting Volcanic Activity. *Elements* 13 (1), 35–40. doi:10.2113/gselements.13.1.35

Tormey, D. (2010). Managing the Effects of Accelerated Glacial Melting on Volcanic Collapse and Debris Flows: Planchon-Peteroa Volcano, Southern Andes. *Glob. Planet. Change* 74 (2), 82–90. doi:10.1016/j.gloplacha.2010.08.003

Walker, G. P. L. (1992). Morphometric Study of Pillow-Size Spectrum Among Pillow Lavas. *Bull. Volcanol.* 54 (6), 459–474. doi:10.1007/bf00301392

Werner, R., and Schmincke, H.-U. (1999). Englacial vs. Lacustrine Origin of Volcanic Table Mountains: Evidence From Iceland. *Bulletin Volcanol.* 60, 335–354.

Wilson, A. M., and Russell, J. K. (2020). Glacial Pumping of a Magma-Charged Lithosphere: A Model for Glaciovolcanic Causality in Magmatic Arcs. *Earth Planet. Sci. Lett.* 548, 116500. doi:10.1016/j.epsl.2020.116500

Wilson, A. M., Russell, J. K., and Quane, S. L. (2019). The Table, a Flat-Topped Volcano in Southern British Columbia: Revisited. *Am. J. Sci.* 319, 44–73. doi:10.2475/01.2019.02